Impact of a deep ozone hole on Southern Ocean primary production

Kevin R. Arrigo,[1] Dan Lubin,[2] Gert L. van Dijken,[1] Osmund Holm-Hansen,[3] and Esther Morrow[2]

Received 16 November 2001; revised 5 December 2002; accepted 25 February 2003; published 22 May 2003.

[1] Field studies show that photosynthesis by Antarctic phytoplankton is inhibited by the increased ultraviolet radiation (UVR) resulting from springtime stratospheric ozone (O_3) depletion. To extend previous observations, a numerical model utilizing satellite-derived distributions of O_3, clouds, sea ice, surface temperature, and phytoplankton biomass was developed to study the hemispheric-scale seasonal effects of a deep Antarctic O_3 hole on primary production in the Southern Ocean. UVR-induced losses of surface phytoplankton production were substantial under all O_3 conditions, mostly due to UVA. However, when integrated to the 0.1% light depth, the loss of primary production resulting from enhanced fluxes of UVB due to O_3 depletion was <0.25%. The loss of primary production is minimized by the strong attenuation of UVR within the water column and by sea ice which is at its peak extent at the time of the most severe O_3 depletion. *INDEX TERMS:* 1615 Global Change: Biogeochemical processes (4805); 1635 Global Change: Oceans (4203); 1640 Global Change: Remote sensing; 4842 Oceanography: Biological and Chemical: Modeling; *KEYWORDS:* ozone, UV-inhibition, Antarctic, phytoplankton production, modeling, remote sensing

Citation: Arrigo, K. R., D. Lubin, G. L. van Dijken, O. Holm-Hansen, and E. Morrow, Impact of a deep ozone hole on Southern Ocean primary production, *J. Geophys. Res.*, *108*(C5), 3154, doi:10.1029/2001JC001226, 2003.

1. Introduction

[2] Springtime depletion of stratospheric ozone (O_3) over Antarctica has increased the transmission of UVB radiation [*Frederick and Snell*, 1988; *Lubin et al.*, 1989; *Stamnes et al.*, 1992] to the sea surface, resulting in measurable inhibition of phytoplankton productivity [*Prézelin et al.*, 1994; *Smith et al.*, 1992; *Holm-Hansen et al.*, 1993; *Neale et al.*, 1998a]. The magnitude of UVB inhibition is a function of phytoplankton sensitivity to UVB radiation [*Smith et al.*, 1992; *Holm-Hansen et al.*, 1993; *Neale et al.*, 1998a], their cumulative exposure to UVB as a function of ocean mixed layer depth (MLD), the speed of vertical mixing [*Neale et al.*, 1998a], the amount of nonliving UVB absorbing material such as chromophoric dissolved organic matter [*Arrigo and Brown*, 1996], and the degree to which the UVR induced damage can be repaired by cellular processes [*Holm-Hansen*, 1997].

[3] Because of the interest in the large-scale ecological effects of the Antarctic O_3 hole (O_3 concentrations <225 Dobson units, DU), attempts have been made to estimate the loss of oceanic photosynthesis resulting from decreased O_3 abundance. Reported daily losses vary from <1 to 12% of the phytoplankton carbon (C) fixation measured under normal O_3 conditions [*Smith et al.*, 1992; *Holm-Hansen et al.*, 1993; *Arrigo*, 1994; *Prézelin et al.*, 1994; *Neale et al.*, 1998a]. In most cases, larger-scale estimates have been based either on simple spatial extrapolations of localized studies or on theoretical calculations that assumed a spatially uniform O_3 concentration representing an idealized O_3 hole. Because current atmospheric radiative transfer models [*Lubin and Jensen*, 1995; *Lubin et al.*, 1998] can calculate fluxes of UVR and visible radiation as a function of O_3 abundance with a high degree of accuracy, it is now possible to use numerical modeling techniques to assess the large-scale effects of stratospheric O_3 depletion on oceanic primary production. Here we present the first hemisphere-scale estimates of the effects of Antarctic O_3 depletion on photosynthetic rates in the Southern Ocean that account for vertical mixing as well as spatial and temporal variation in O_3 abundance, sea ice cover, cloudiness, wind speed, MLD, and phytoplankton chlorophyll *a* (Chl *a*).

2. Methods

[4] To determine the effects of a severe Antarctic O_3 hole on rates of primary production throughout the Southern Ocean, a model of phytoplankton photosynthesis was forced using downwelling irradiance computed using O_3 fields from a low O_3 year (1992) [*Herman and Larko*, 1994] and the results compared to parallel simulations made using O_3 data from a pre-O_3 hole year (1979), having held all other variables constant. Unless otherwise specified, results

[1]Department of Geophysics, Stanford University, Stanford, California, USA.
[2]California Space Institute, Scripps Institution of Oceanography, University of California, San Diego, La Jolla, California, USA.
[3]Marine Research Division, Scripps Institution of Oceanography, University of California, San Diego, La Jolla, California, USA.

0148-0227/03/2001JC001226$09.00

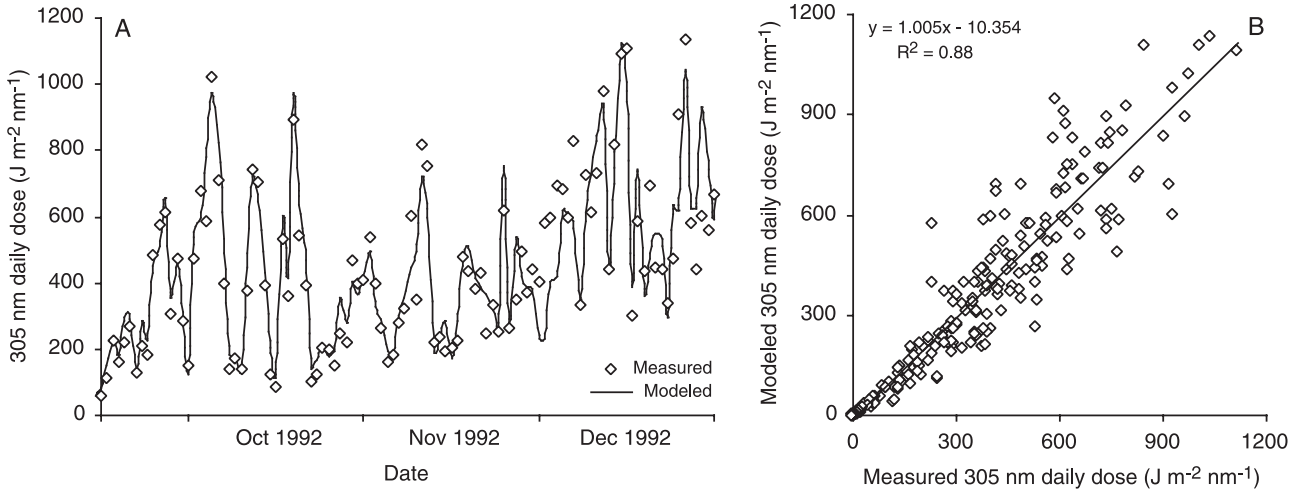

Figure 1. Comparison of surface daily UV (305 nm) doses predicted by the model and measured at Palmer Station, Antarctica (as part of the NSF Office of Polar Programs UV Spectroradiometer Network) for the year 1992. The regression equation of predicted daily UV (305 nm) dose versus observed has an R^2 of 0.88 and a slope of 1.005. Other wavelengths exhibited similar agreement (data not shown).

are expressed as the percent change in production between 1979 and 1992, with 1979 being the baseline. The accepted definition of the Southern Ocean is that it includes all marine waters south of the Antarctic Polar Front. The location of the Polar Front, however, varies geographically from 47°S to 60°S and also varies seasonally to some extent. Our model has thus used an operationally simpler definition of the Southern Ocean as all waters south of 50°S. The circular areas in Figures 2, 6, 8–10, and 20 show regions south of 50°S. For the O_3 hole year simulations, data on stratospheric O_3, cloud optical depth, and sea ice concentrations from 1992 were used. The phytoplankton production during the pre-O_3 hole period was simulated using this same forcing data set but substituting the 1992 O_3 time series with O_3 data collected in 1979. Sea surface temperature (SST) and Chl *a* fields also were common to both years and were determined from *Levitus and Boyer* [1994] climatologies and Sea-viewing Wide Field-of-view Sensor (SeaWiFS) climatologies (1997–2001), respectively. The model was run from 1 August through 31 December of both years, the season of maximum O_3 depletion over Antarctica.

2.1. Model Description

2.1.1. Atmospheric Radiation

[5] For both 1979 and 1992, surface irradiance spectra were retrieved daily at local noon and at midnight using TOMS measurements of total column O_3 and scene reflectivity using a modified version of a detailed atmospheric radiative transfer model [*Lubin and Jensen*, 1995; *Lubin et al.*, 1998]. The spatial resolution of these retrievals (~100 km) is identical to that of the gridded TOMS data. A computationally efficient delta-Eddington radiative transfer formulation [*Joseph et al.*, 1976; *Briegleb*, 1992] was used to estimate the cloud optical depth from the 380 nm Lambert-equivalent scene reflectivity retrieved from the Nimbus-7 TOMS [*Eck et al.*, 1987; *Herman et al.*, 1999]. The UVR surface albedo was specified in this optical depth estimation from an empirical relationship involving sea ice concentration, modeled from the work of *Allison et al.* [1993], as follows: (1) For open ocean, the UVR surface albedo is set at 0.05, (2) for 100% sea ice coverage, the UVR surface albedo is set at 0.80, and (3) for partial sea ice coverage, the UVR surface albedo varies linearly with ice fraction, between the two extremes. The sea ice concentrations are determined from Special Sensor Microwave Imager (SSM/I) satellite data [*Cavalieri et al.*, 1997] gridded to the TOMS data. The 380 nm cloud optical depth retrievals were used with the TOMS total column O_3 and the UVR surface albedo as input to a forward delta-Eddington algorithm [*Lubin and Jensen*, 1995] to calculate the downwelling irradiance (280 to 700 nm) at the ocean surface, with a spectral resolution of ~5 nm. To estimate spectral irradiance at 1-hour intervals throughout the daylight period, a sine function was then fit to the spectral irradiance retrievals at noon and midnight. These hourly values were integrated over 24 hours to obtain highly accurate estimates of the daily dose of spectral irradiance at each wavelength (Figure 1). A potential source of error is the use of one daily observation of cloud optical depth (local noon) to derive a daily integrated dose. If there is significant diurnal variability in cloud cover, some important climate system variability may be overlooked. However, *Lubin et al.* [1998] showed, by intercomparison of TOMS local noon UVR retrievals with UVR retrievals based on diurnal cloud information from the Earth Radiation Budget Experiment (ERBE), that in most regions the diurnal variability due to solar elevation is more significant in determining the daily UVR dose than diurnal cloud variability. Regions where neglect of diurnal cloud variability can result in errors of more than a few percent tend to be confined to the tropics (e.g., regions of deep convection). In contrast, the maritime Antarctic is characterized by extensive storm systems that bring overcast sky conditions for many days, followed by quiescent or cloud-free events of shorter duration. In this region, daily cloud variability (captured by the TOMS reflectances) is more significant than diurnal variability.

2.1.2. Model Grid

[6] All surface fields (SST, sea ice concentration, downwelling irradiance, MLD, Chl *a*) were gridded to the SSM/I grid, with an approximate horizontal resolution of 25 km. The vertical resolution of the model grid varied with depth, decreasing exponentially from 0.1 m at the surface to 4.6 m at 200 m, with a total of 100 depths between 0 and 200 m. Chl *a* was taken to be vertically homogeneous from the ocean surface to the MLD and equal to the concentration determined from SeaWiFS. Below the MLD, Chl *a* was assumed to decrease exponentially, the rate of decrease being a function of surface Chl *a* concentration [*Arrigo et al.*, 1998a]. In this way, higher surface Chl *a* is associated with a more rapid decline in Chl *a* with depth below the MLD. The detrital absorption at each depth was calculated as a function of Chl *a* according to the relationship given in *Arrigo et al.* [1998a]. Profiles of downwelling spectral irradiance were estimated from vertical profiles of Chl *a* and detrital absorption, as well as from attenuation by chromophoric dissolved organic matter (CDOM), which was held constant with depth (see below). Temperature was assumed to be uniform throughout the upper 200 m and equal to the SST from *Levitus and Boyer* [1994].

2.1.3. Surface Reflection

[7] The downwelling spectral irradiance (λ = 280–700 nm) at time t just penetrating the ocean surface, $E_d(\lambda, 0^-, t)$ was calculated as

$$E_d(\lambda, 0^-, t) = (1 - \alpha_d)E_{dd}(\lambda, 0^+, t) + (1 - \alpha_i)E_{di}(\lambda, 0^+, t), \quad (1)$$

where E_{dd} and E_{di} are the direct and indirect radiation components, α_d and α_i are the specular reflectance for direct and indirect radiation, and 0^- and 0^+ refer to the positions just below and just above the ocean surface, respectively. For the sake of simplicity, λ and t will be dropped from further equations of irradiance attenuation. Following the approach of *Gregg and Carder* [1990], surface reflectance (α) was divided into direct (d) and diffuse or indirect (i) components, both of which are the sum of specular reflection (r) and reflectance from sea foam (f),

$$\alpha_d = \alpha_{dr} + \alpha_f \quad (2a)$$

$$\alpha_i = \alpha_{ir} + \alpha_f. \quad (2b)$$

[8] Foam reflectance (α_f) was modeled as a function of wind stress (W^2) as described by *Gregg and Carder* [1990]. The values for α_i, α_{ir}, and α_f are independent of solar zenith angle (θ) while the specular reflection (α_{dr}) for a flat ocean (wind speed, W, is <2 m s^{-1}) was calculated from θ in accordance with Fresnel's law,

$$\alpha_{dr} = 0.5\left[\frac{\sin^2(\theta - \theta_w)}{\sin^2(\theta + \theta_w)} + \frac{\tan^2(\theta - \theta_w)}{\tan^2(\theta + \theta_w)}\right], \quad (2c)$$

where θ_w is the refracted angle in water. At wind speeds above 2 m s^{-1}, α_{dr} was taken to be an empirical function of W [*Gregg and Carder*, 1990]. For diffuse radiation, α_{dr} was set to 0.066 and 0.057, respectively, at wind speeds below and above 4 m s^{-1} [*Burt*, 1954].

2.1.4. In-Water Optics

[9] Spectral irradiance penetration through the water column was estimated using the Beer-Lambert law,

$$E_d(z) = E_d(0^-)^{e^{-K_d(z)z}}, \quad (3)$$

where $K_d(z)$ is the diffuse attenuation coefficient (m^{-1}) for downwelling irradiance at depth z. $K_d(z)$ was partitioned into components describing attenuation by pure water (w), phytoplankton (p), detritus (Det) and CDOM such that

$$K_d(z) = K_{dw} + K_{dp}(z) + K_{dDet}(z) + K_{dCDOM}(z). \quad (4a)$$

The apparent optical property K_d is related to its constituent inherent optical properties absorption (a) and backscattering (b_b) through the quantity μ, the mean cosine for downwelling irradiance. Pure water K_{dw} was therefore calculated as

$$K_{dw}(z) = \frac{b_{bw}(z) + a_w(z)}{\mu}, \quad (4b)$$

where b_b and a are given in *Smith and Baker* [1981]. $K_{dp}(z)$ was computed as

$$K_{dp}(z) = \frac{b_{bp}(z) + a_p^*(z)Chl\ a(z)}{\mu}, \quad (4c)$$

where $b_{bp}(z)$ is the backscatter (m^{-1}) by microalgae computed according to the procedure described by *Sathyendranath and Platt* [1989], $a_p^*(\lambda)$ (m^2 mg Chl a^{-1}) is the pigment-specific absorption coefficient for microalgae, and Chl *a* is the chlorophyll *a* concentration (mg m^{-3}). The coefficient μ for diffuse irradiance was taken from *Sathyendranath and Platt* [1989] and for direct irradiance is equal to $\cos(\theta_w)$. $K_{dDet}(z)$ is computed from the absorption by detritus as

$$K_{dDet}(z) = \frac{a_{Det}(440, z)e^{S_1(\lambda - 400)}}{\mu}, \quad (4d)$$

where $a_{Det}(440, z)$ = 0.006 Chl $a(z)$ and $S_1 = -0.0143$ [*Arrigo et al.*, 1998a]. Finally, attenuation by CDOM is calculated as

$$K_{dCDOM}(z) = \frac{a_{CDOM}(400, z)e^{S_2(1 - 400)}}{\mu}, \quad (4e)$$

where $a_{CDOM}(400, z)$ = 0.0285 and $S_2 = -0.012$ [*Mitchell and Holm-Hansen*, 1991; *Arrigo et al.*, 1998a].

2.1.5. Phytoplankton Production

[10] Profiles of temperature, spectral irradiance, and Chl *a* were used as input to the phytoplankton primary production model of *Arrigo et al.* [1998b], which was modified to account for inhibition of photosynthesis by UVR. UVR inhibition was calculated as a function of cumulative daily UVR exposure, taking into account the effects of vertical mixing of the upper ocean [*Neale et al.*, 1998a], daily changes in MLD, and wavelength-specific sensitivity of phytoplankton production to ambient UVR [*Neale et al.*, 1998b], referred to as the biological weighting function

(BWF). We used the BWF derived by *Neale et al.* [1998b] for Antarctic phytoplankton from Station R (30 October 1993, deep mixed layer) in the Weddell-Scotia Confluence. Although the applicability of this BWF to other Antarctic waters is unknown, a sensitivity analysis is presented near the end of this paper showing that our conclusions are not very sensitive to the BWF chosen.

[11] In the modified model, the rate of primary production (PP, g C m^{-3} d^{-1}) at depth z and time t is calculated as

$$PP(z,t) = G(z,t)(C/Chla)B_{\text{eff}}(z,t), \tag{5}$$

where G is the phytoplankton growth rate (d^{-1}) calculated from temperature and light availability as described by *Arrigo et al.* [1998b], $C/Chla$ is the phytoplankton C:Chl a mass ratio (50), and B_{eff} is the effective phytoplankton concentration (mg Chl a m^{-3}) which includes the effect of UVR inhibition (see below) as defined by *Neale et al.* [1998a]. G is modeled as the product of the temperature-dependent maximum rate and a light limitation term such that

$$G(z,t) = G_0\ e^{kT(z)}\left(1 - e^{-PUR(z,t)/E_k}\right), \tag{6}$$

where G_0 is 0.59 (d^{-1}) and k is 0.0633 ($°C^{-1}$) [*Eppley*, 1972], T is temperature (°C), PUR is the photosynthetically usable radiation (μEin m^{-2} s^{-1}), and E_k (μEin m^{-2} s^{-1}) is the spectral photoacclimation parameter as described by *Arrigo et al.* [1998b]. PUR was calculated from downwelling spectral irradiance as described by *Morel* [1978] using the absorption spectrum for Antarctic phytoplankton shown in Figure 18a in section 3.3.6 [*Arrigo et al.*, 1998a].

[12] The formulation by *Neale et al.* [1998a] describing the effect of cumulative exposure to UVR was used to simulate UVR inhibition of primary production. This formulation is based on the physiological inactivation of algal biomass (effective biomass, B_{eff}) and has the added advantage of being able to include the effect of vertical mixing on estimates of UVR inhibition. At dawn, $B_{\text{eff}}(z, t)$ is set equal to Chl $a(z, t)$. Throughout the day, $B_{\text{eff}}(z, t)$ is progressively reduced by UVR exposure according to the relationship

$$B_{\text{eff}}(z,t) = B_{\text{eff}}(z, t - \Delta t)\ e^{-H_{inh}(z,t)}, \tag{7a}$$

where

$$H_{\text{inh}}(z,t) = \int_{t=0}^{\Delta t} \int_{\lambda=280\ nm}^{700\ nm} \varepsilon_{\text{H}}(\lambda,z,t)E_{\text{d}}(\lambda,z,t)d\lambda dt, \tag{7b}$$

and Δt is the time step of the model (5 min), and ε_{H} is the BWF. According to this formulation, B_{eff} declines with each successive Δt, diminishing most rapidly near the sea surface where UVR is greatest. To simulate vertical mixing within the mixed layer, at a specified time (T_{mix}), B_{eff} is averaged over the MLD and this mean value is applied uniformly to each layer within the MLD. T_{mix} can be adjusted to allow for rapid (small T_{mix}) or slow (large T_{mix}) mixing rates within the mixed layer. Reduction of B_{eff} then continues until the beginning of the next day at which time $B_{\text{eff}}(z, t)$ is again set equal to the satellite-derived Chl a profile for that day, simulating complete recovery each day after UVR exposure.

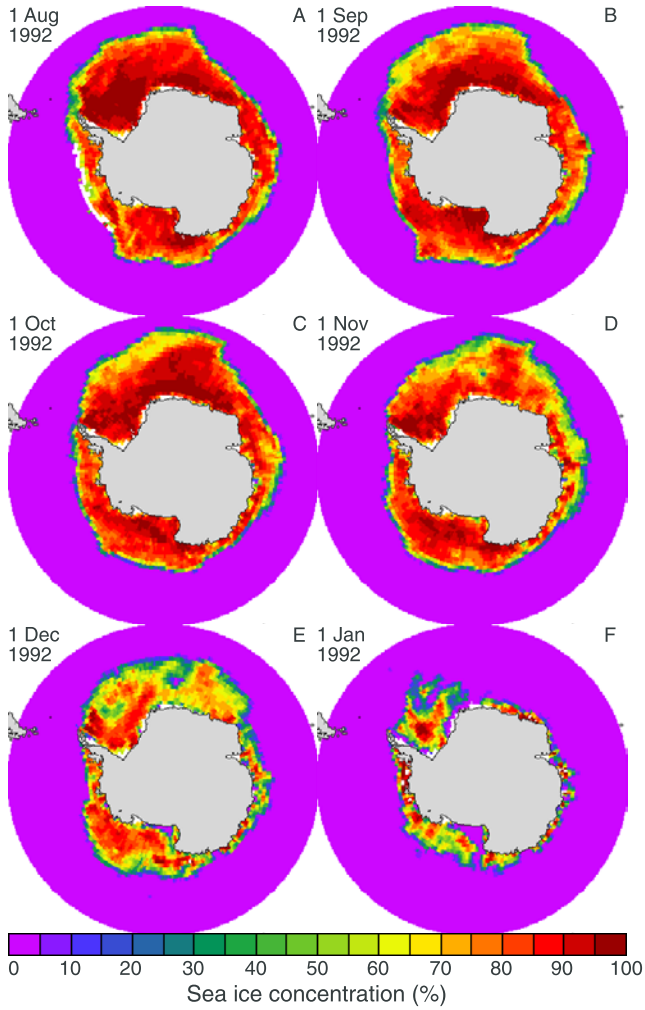

Figure 2. Sea ice distribution within our study area on the first day of each month during 1992 as determined by SSM/I.

2.2. Model Input Data

2.2.1. Sea Ice

[13] Sea ice concentrations for the year 1992 were determined daily using Special Sensor Microwave/Imager (SSM/I) data obtained from the National Snow and Ice Data Center (NSIDC). Sea ice extent increased slightly between August (Figure 2a) and September 1992, where it reached a maximum coverage of 17.1 × 10^6 km^2 (Figure 2b). After September, sea ice concentration and extent began to decline as solar insolation and atmospheric temperatures began to increase with the approach of austral spring. This decline in sea ice continued throughout our study period, reaching a minimum extent of 4.4 × 10^6 km^2 on 1 January 1993 (Figure 2f). Even in early summer, however, sea ice cover was still substantial in the Weddell, Bellingshausen-Amundsen, and Ross seas (Figure 2f).

2.2.2. Sea Surface Temperature

[14] SST, which is used in the calculation of phytoplankton production rate, was specified using the monthly clima-

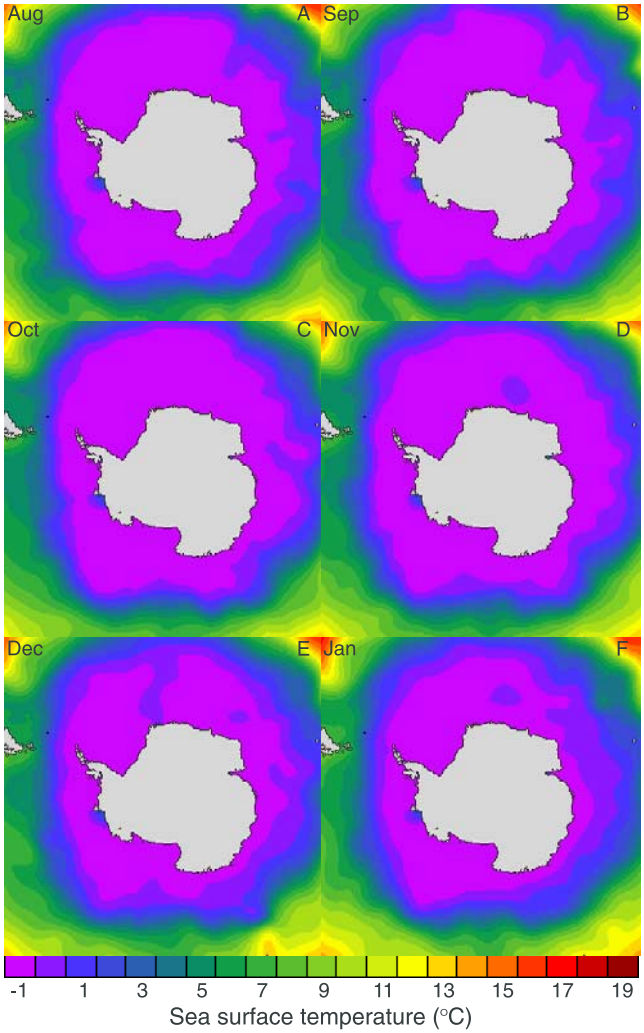

Figure 3. Monthly climatological sea surface temperature distributions [*Levitus and Boyer*, 1994] within our study area.

tologies of *Levitus and Boyer* [1994]. These data were then interpolated to obtain daily SST fields that were assumed to apply to all depths within the upper mixed layer. In general, SST climatologies exhibit little change between early August (Figure 3a) and late December (Figure 3f). In some places, the 0°C isotherm constricts somewhat between winter and early summer, moving closer to the Antarctic continent. Regardless of season, however, most of the waters in our study area range in temperature from −1.8°C to +4°C. As a result of these relatively small temperature differences, maximum phytoplankton production rates would be expected to vary spatially by approximately 50%.

2.2.3. Chlorophyll *a*

[15] Chl *a* concentrations were determined from data collected by SeaWiFS and archived at the Goddard DAAC. Climatological maps of Chl *a* were constructed by calculating 10-day binned mean fields (e.g., 1–10 December, 11–20 December, 21–31 December) using all GAC (4 km) data available between 1997 and 2001. In order to save power, SeaWiFS only collects data over a limited portion of each orbit. As a result, in late austral winter (e.g., August), SeaWiFS does not routinely collect data south of 55°S, focusing its efforts on waters of the polar north instead. Hence the large region of missing data (white area) in Figure 4a. After early September, however, SeaWiFS records data over more southerly waters, and all of the open water north of the sea ice edge is sampled (Figure 4b).

[16] In August and September, Chl *a* concentrations in our study area were relatively uniform at approximately 0.1 mg m^{-3} (Figures 4a and 4b). By October, the spring phytoplankton bloom had begun in isolated areas near the marginal ice zone (MIZ) and along the Polar Front (Figure 4c). Although Chl *a* concentrations over most of the Southern Ocean remained near 0.1 mg m^{-3}, Chl *a* reached as high as 3–5 mg m^{-3} in the few phytoplankton blooms. During the months of November (Figure 4d) and December (Figure 4e), Chl *a* concentrations around most of Antarctica were in excess of 0.5 mg m^{-3} and exceeded 1 mg m^{-3} over wide areas. Coastal

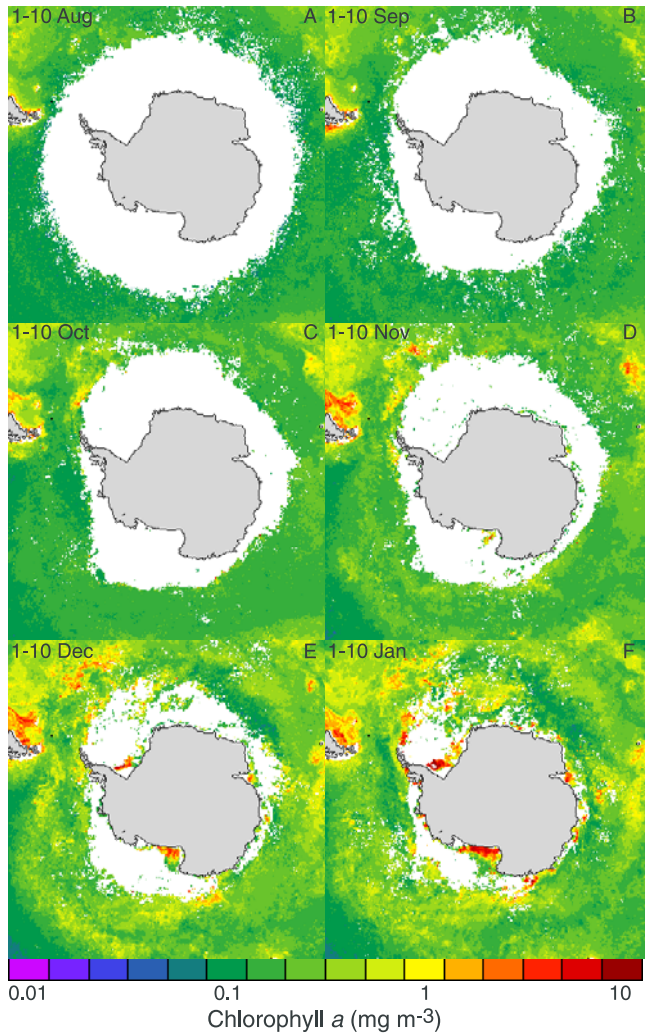

Figure 4. Temporal changes in climatological Chl *a* distribution (1997–2001) within our study area as determined by SeaWiFS. White areas indicate where data were not available due to satellite data collection patterns (in the case of Figure 4a), cloud cover (only minor losses), and/or sea ice cover.

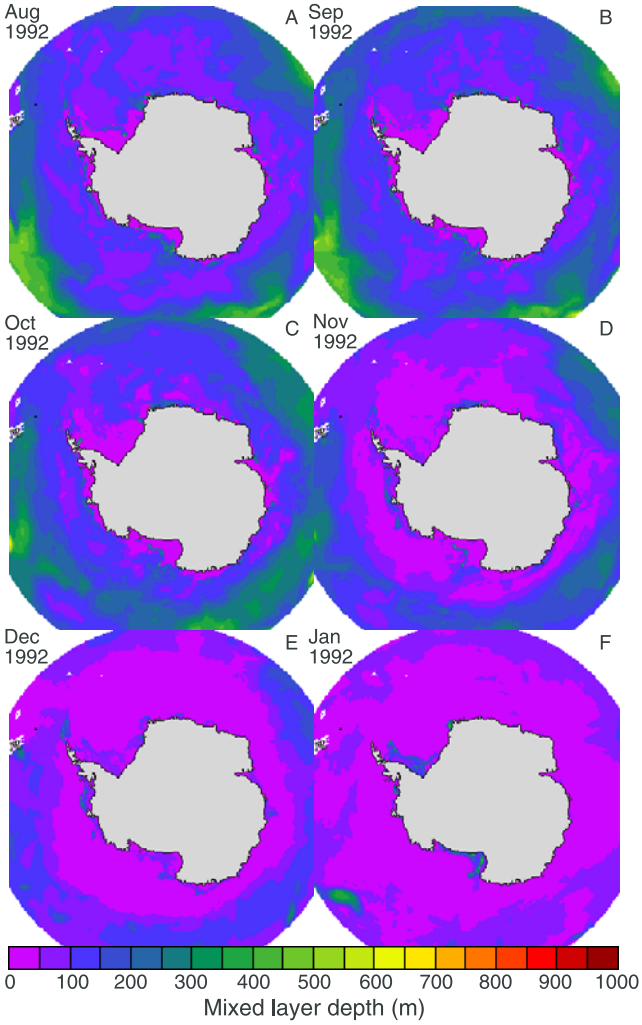

Figure 5. Temporal variations in mixed layer depth distribution within our study area during 1992 determined by *Markus* [1999].

blooms had begun to form by this time, often associated with major polynya systems, such as in the Ross Sea, Prydz Bay, and the Weddell Sea. In some areas, concentrations in excess of 5 mg m^{-3} extended for >100,000 km^2.

2.2.4. Mixed Layer Depth

[17] The MLD was estimated weekly for the year 1992 using the model of *Markus* [1999]. This bulk mixed layer model of the Southern Ocean was forced by climatological European Centre for Medium-Range Weather Forecast (ECMWF) near-surface air temperatures and winds, and by sea ice concentrations from SSM/I.

[18] During austral autumn and winter, surface cooling over much of the Southern Ocean leads to destabilization of surface waters and convective overturn which persists through to early austral spring. Deep mixing is further facilitated by strong winds over areas of open water. In these areas during August, MLD typically exceeds 200 m (Figure 5a), resulting in mean irradiance levels in surface waters that are too low for net photosynthesis. Throughout the spring and early summer, increased solar insolation and melting sea ice reduces MLD dramatically, such that by November (Figure 5d) and December (Figure 5e), MLDs of <50 m are widespread. Irradiance levels in these waters are sufficiently high to support net photosynthesis, hence the beginning of the phytoplankton blooms observed in the SeaWiFS imagery (Figure 4).

2.2.5. Stratospheric O_3 Concentration

[19] O_3 concentrations for 1979 and 1992 were specified using data from the Total Ozone Mapping Spectrometer (TOMS), obtained from the TOMS project at NASA Goddard Space Flight Center.

[20] During 1979, stratospheric O_3 concentrations remained above 300 DU throughout the Antarctic for most of the year (Figure 6), averaging >330 DU (Figure 7a). O_3 concentrations were reduced somewhat during September, when O_3 fell to <220 DU over a very small area (Figure 6c), although the mean O_3 concentration was still >320 DU (Figure 7a). Between October and November 1979, mean O_3 levels increased by 13% (Figure 7a) and values greater than 500 DU covered a wide area (Figure 6e). Levels remained high throughout November and December, averaging ~380 DU (Figure 7a) and with maximum values <450 DU (Figures 6i and 6k).

[21] In contrast, O_3 concentrations in 1992 were greatly reduced from their 1979 levels. In early August, O_3 concentrations in our study area averaged slightly more than 320 DU (Figure 7a). However, between early August (Figure 6b) and late September (Figure 6d), the size of the O_3 hole (defined as the region with O_3 <225 DU) had increased to $>20 \times 10^6$ km^2 (Figure 7b), with mean O_3 levels of 270 DU (Figure 7a). The minimum discrete O_3 value of that year (124 DU) was measured on 10 October over the Antarctic continent near the Weddell Sea. As the O_3 hole began to shrink in early October 1992 (Figure 7b), mean O_3 concentration steadily increased to approximately 315 DU (Figure 7a). Even after the 1992 O_3 hole had disappeared completely (Figure 7b), mean O_3 levels were still 11% below levels measured at the same time in 1979 (Figure 7a).

3. Results

3.1. Fluxes of UVB, UVA, and PAR Over Open Water

3.1.1. UVB (280–320 nm)

[22] Noontime fluxes of surface UVB in early August were low in both 1979 and 1992, ranging from <0.5 W m^{-2} at 50°S down to almost zero near the Antarctic continent (Figures 8a and 8b), averaging approximately 0.16 W m^{-2}. Differences in mean UVB between 1979 and 1992 at this time were <1%. UVB distributions on 1 September 1992 exhibited an asymmetric pattern (Figure 8d), with the highest values located over the northern Weddell Sea where O_3 levels were lowest (Figure 6d). The 1979–1992 differences in UVB flux at this time were greatest in the Pacific sector, consistent with the observed reduction in O_3.

[23] As solar elevation increased in early spring, UVB flux increased as well, averaging 0.80 W m^{-2} and 0.92 W m^{-2} on 1 October in 1979 and 1992, respectively (a difference of 15%), with levels as high as 1.5 W m^{-2} at the most northerly latitudes of our study area. Although the O_3 hole peaked in size at this time (Figure 7b) and mean O_3 levels were at their seasonal minimum (Figure 7a), UVB levels continued to rise as a result of ever increasing solar insolation. Mean surface UVB reached its seasonal max-

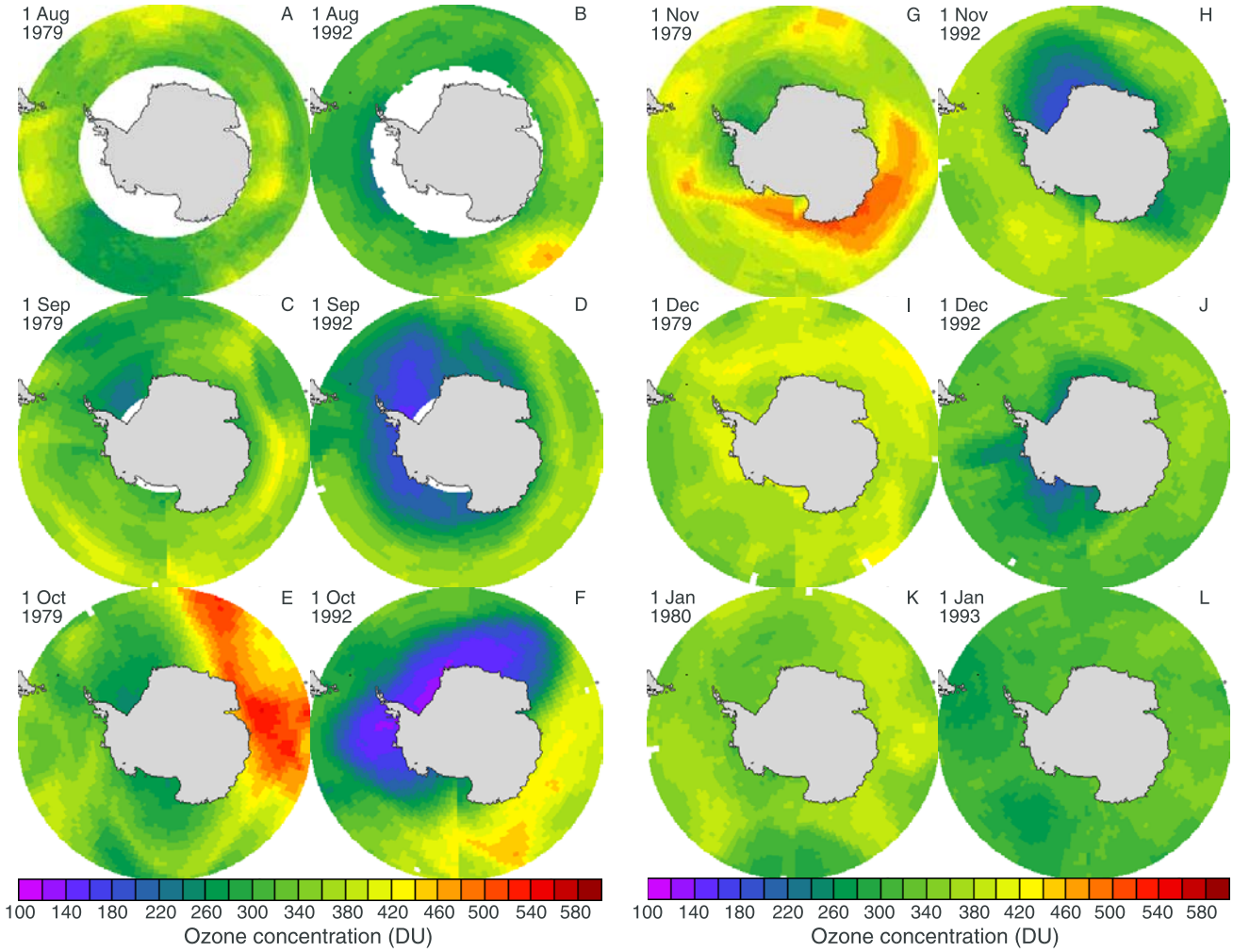

Figure 6. Temporal variations in ozone distribution for 1979 and 1992 within our study area as determined by the TOMS.

imum near the summer solstice in both 1979 (1.47 W m^{-2}) and 1992 (1.67 W m^{-2}), exhibiting peak values of 2.53 W m^{-2} and 2.72 W m^{-2}, respectively. After the O_3 hole disappeared in early December, mean UVB was still 15% higher in 1992 than in the same time period of 1979.

[24] The magnitude of the surface UVB flux is controlled not only by O_3 concentration, but by cloud optical depth as well (Figure 9b). The effects of O_3 abundance (Figure 9a) are clearly evident in the distribution of UVB estimated for 4 October 1992 (Figure 9c), with low UVB fluxes generally corresponding to regions of high O_3. However, the large-scale correspondence between O_3 and UVB is modified substantially at smaller scales by the presence of clouds. For example, the areas of the lowest UVB flux on 4 October 1992 (Figure 9c) are associated with high cloud optical depth, and are nearly independent of O_3 levels. Even in regions under the influence of the O_3 hole (e.g. between the Antarctic Peninsula and the tip of South America), UVB is greatly reduced by the presence of clouds.

3.1.2. UVA (320–400 nm) and PAR (400–700 nm)

[25] In general, the flux of UVA and PAR (Figure 10) are approximately 20 and 150 times greater, respectively, than the flux of UVB, due to differences in incoming solar radiation at the top of the atmosphere and to greater absorption of UVB by stratospheric O_3. Because O_3 absorbs very little UVA or PAR, spatial and temporal variation in their downwelling flux is controlled predominantly by solar zenith angle and cloud cover. The effect of solar zenith angle on the magnitude of surface UVA and PAR is expressed both as a greater than two-fold latitudinal increase in noontime flux between 80°S and 50°S and a greater than three-fold increase in noontime flux between late winter and early summer.

[26] Superimposed on this latitudinal and temporal trend in the surface flux of UVA and PAR are changes due to cloud cover. Under heavy clouds, UVA and PAR can be reduced by as much as 80–90%, although a 50% reduction is more typical. Taking into account the effect of clouds and latitude, the noontime flux of UVA and PAR in early August averaged 11 W m^{-2} and 110 W m^{-2}, respectively, increasing to 38 W m^{-2} and 330 W m^{-2}, respectively, at the summer solstice.

3.2. Primary Production

3.2.1. Productivity at Station A (59.19°S and 56.89°E) on 4 October

[27] Because results of the model are more easily understood at smaller spatial and temporal scales, particularly

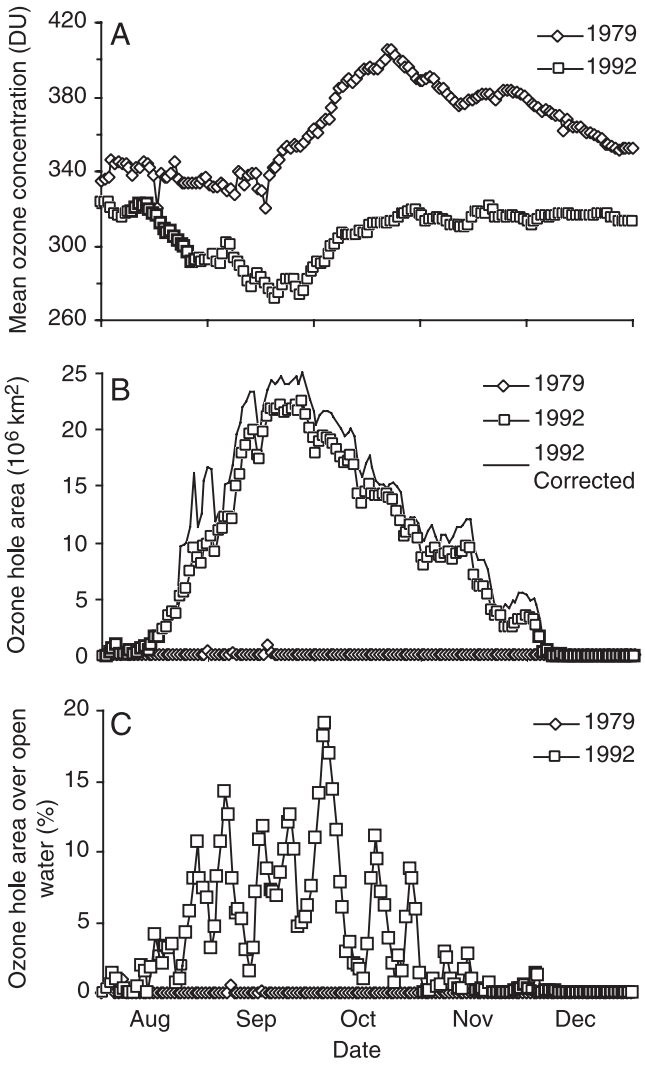

Figure 7. Daily variations in (a) mean ozone concentration south of 50°S for 1979 and 1992 determined from TOMS data, (b) size of the ozone hole (ozone <225 DU) determined from TOMS data for 1979 and 1992 (there is a gap in TOMS data at the south pole (see Figures 6a–6d) and the "1992 corrected" represents an upward correction in ozone hole area to account for that portion of the ozone hole that is located over the data gap), and (c) percent of the ozone hole over open water (defined as sea ice concentration <50% from SSM/I) for 1979 and 1992.

with respect to the depth-dependent responses of the phytoplankton to UVR, we have chosen to initially present model results for a specific day and location. The location of Station A was chosen so as to maximize the O_3 differences between 1979 (199 DU) and 1992 (546 DU) (Figure 11a), thus providing a good example of the effect that changing O_3 concentration can have on phytoplankton production. Chl *a* on 4 October at Station A was relatively low at approximately 0.2 mg Chl *a* m^{-3} (Figure 11b) and SST was −0.48°C (Figure 11b); cloud cover was moderate (Figure 11c) and the MLD was 220 m (Figure 11c).

[28] The product of the BWF and spectral UVR integrated from 280 to 400 nm, H_{inh} (equation (7b)), is used to calculate the effective phytoplankton biomass, B_{eff} (equation (7a)), and ultimately, the degree of UVR inhibition of primary production (equation (5)). H_{inh} varies with time and depth, being highest at noon at the ocean surface and diminishing rapidly with time and depth (Figure 12a) as UVR is attenuated by seawater, CDOM and suspended particulates. At noon on 4 October, H_{inh} calculated at the ocean surface as a function of total UVR (UVA+B) was 30% greater in 1992 than in 1979, increasing from 0.01 to 0.13, due primarily to an increase in the contribution from UVB (Figure 12a). In the upper 20 m, the fraction of H_{inh} resulting from the flux of UVB was 2 to 2.4 times greater in 1992 than in 1979 whereas the contribution by UVA was relatively unchanged. However, the high levels of total H_{inh} (from UVA + B) in both years were due mostly to UVA, which was responsible for 82–95% of total H_{inh} in the topmost 20 m in 1979. The relative role of UVA was diminished somewhat in 1992 due to the lower O_3 and relatively greater flux of UVB. Nevertheless, UVA still accounted for 66–90% of total H_{inh} in the upper 20 m in 1992.

[29] The effect of depth-dependent changes in H_{inh} can be seen in profiles of B_{eff} between noon, just after the simulated mixing over the MLD, and 15:00 hours, the next mixing of the water column (i.e., T_{mix} = 3 hours) during these simulations. Within 0.5 hours of mixing at noon on 4 October 1979, B_{eff} at the surface (Figure 12b) had been reduced by nearly 46% due to UVR, from 0.18 to 0.10 mg Chl *a* m^{-3}, although this reduction became much less severe with depth. By 14:30 hours B_{eff} was 0.047 mg Chl *a* m^{-3} at the surface, but showing evidence of UVR influence down to 30 m. At 15:00 hours, the water column was mixed down to the 220 m MLD (Figure 11c) and the B_{eff} averaged over this depth interval was reduced from 0.184 at 12:00 hours to 0.175 at 15:00 hours, a decline of 5.0% over 3 hours.

[30] Changes in B_{eff} between noon and 15:00 hours were somewhat greater on 4 October 1992 (Figure 12c), due to the higher levels of UVR, particularly UVB. Thirty minutes after mixing at noon, B_{eff} at the surface was reduced from 0.183 to 0.083, a decline of 55%. By 14:30 hours, B_{eff} at the surface in the 1992 simulation was 57% lower than at the same point in 1979, although this difference rapidly diminished with depth, amounting to only 1% at 20 m. After water column mixing at 15:00 hours, B_{eff} in 1992 had declined to 5.14% below its noontime level, compared to the 5.07% decline during the same time interval in 1979. The primary reason for the small change in B_{eff} at 15:00 hours between 1979 and 1992 is the depth of the mixed layer. Although the difference in B_{eff} between 1979 and 1992 is substantial in the upper water column, after mixing to 220 m, this difference gets largely averaged out.

[31] Calculation of H_{inh} and B_{eff} continue throughout the light cycle (at 5-min intervals), and the daily production resulting from these calculations can be seen in Figure 12d. Daily production is most strongly inhibited in those simulations where phytoplankton were allowed to respond to both UVA and UVB (UVA + B). Loss of production in surface waters (relative to the simulation where UVR was removed) varied from 59% in 1979 to 66% in 1992. Simulations where phytoplankton only responded to UVA were inhibited nearly as strongly in surface waters, with a 54% and 55% loss in production in 1979 and 1992,

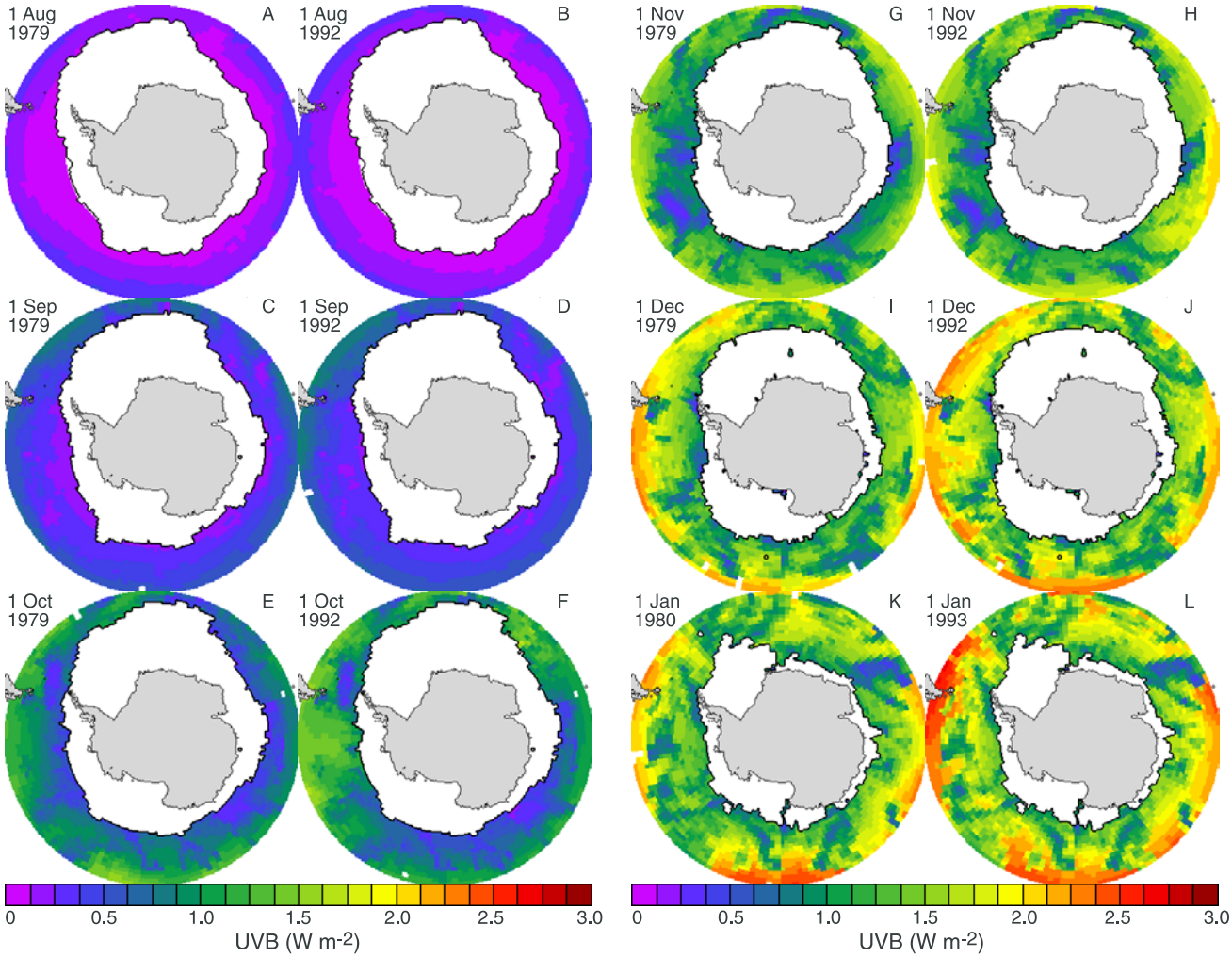

Figure 8. Temporal variations in modeled downwelling surface UVB at local noon for 1979 and 1992. White areas represent sea ice covered regions.

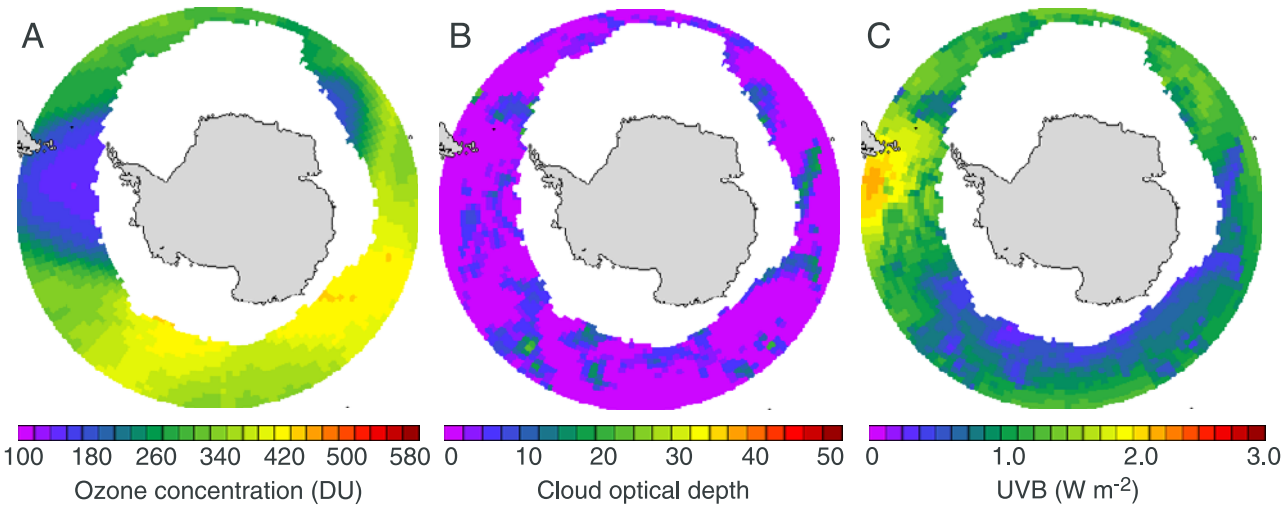

Figure 9. Maps of (a) ozone concentration, (b) cloud optical depth, and (c) downwelling surface UVB at local noon on 4 October 1992 showing how both cloud cover and ozone abundance have a strong impact on the flux of UVB. White areas represent sea ice covered regions.

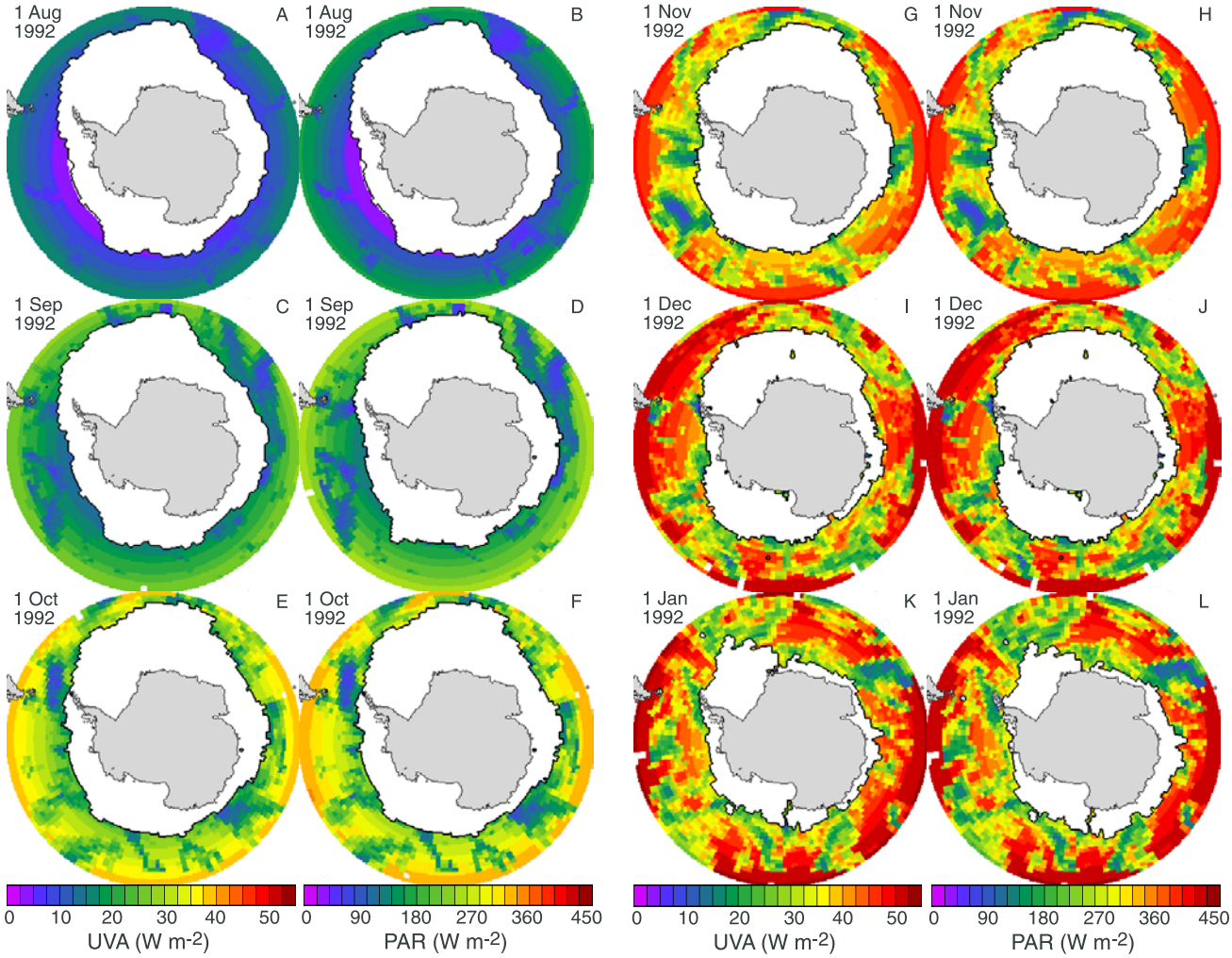

Figure 10. Temporal variations in modeled downwelling surface UVA and PAR at local noon. Because O_3 absorption has a very minor impact on transmission of UVA and PAR, and because the only difference between the 1979 and 1992 simulations was the stratospheric O_3 abundance, maps of UVA and PAR for the 2 years are virtually indistinguishable. Therefore, to save space, data for 1992 only are shown. White areas represent sea ice covered regions.

respectively. UVB alone resulted in the lowest loss of surface production (37%), but the largest production difference between 1979 and 1992 (19%) from the no-UVR simulations.

[32] Although inhibition by UVR was high in surface waters, when integrated over the water column, the degree of UVR inhibition was reduced dramatically. Differences in depth-integrated production between the no UVR and the UVA+B cases were 17% and 19% for 1979 and 1992, respectively. The aggregate effect of the 4 October 1992 O_3 hole was to lower depth-integrated primary production by 1.7% below 4 October 1979 levels. Interestingly, if UV effects are ignored entirely, then primary production in 1992 is predicted to be 0.4% greater than in 1979, due to increased transmission of PAR at the reduced 1992 O_3 levels.

3.2.2. Seasonal Cycle of Production at Station A

[33] Losses of primary production resulting from UVR inhibition increased between winter and summer at Station A (Figure 13) in response to seasonal increases in solar insolation. The impact of increasing solar insolation is seen most clearly in the loss of production at the ocean surface around noon (Figure 13b), which, like solar insolation, increased most rapidly between August and October. At the peak of the O_3 hole between September and late December, the loss of productivity due to UVR at the ocean surface increased from 60% to approximately 90%, consistent with in situ measurements of UVR inhibition in surface waters of the Southern Ocean which range from 65 to 88% [*Helbling et al.*, 1992; *Smith et al.*, 1992, *Holm-Hansen et al.*, 1993; *Vernet et al.*, 1994; *Boucher and Prézelin*, 1996]. When integrated over the entire water column, losses of primary production also varied with the seasonal solar cycle (Figure 13c), but were modified by changes in the MLD, which shoaled between early October and late December (Figure 11c). This reduction in MLD had the effect of concentrating the phytoplankton community closer to the ocean surface where UVR inhibition is more severe. As a consequence, the loss of total water column production increased more rapidly between November and January,

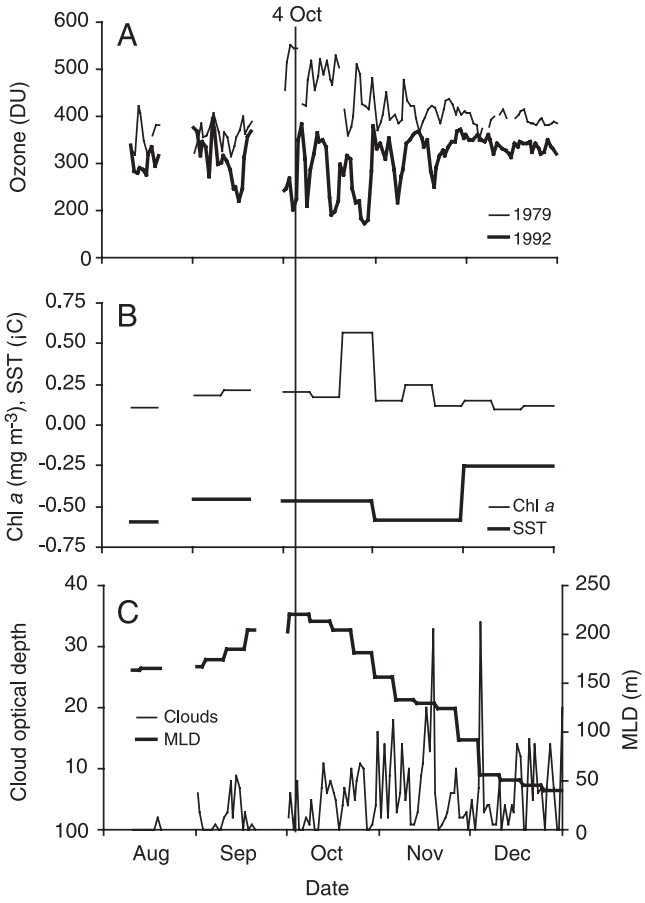

Figure 11. Temporal variations in (a) ozone concentration in 1979 and 1992, (b), Chl *a* concentration and sea surface temperature (SST), and (c) cloud optical depth and mixed layer depth (MLD) on October 4 at Station A (59.19°S and 56.89°E).

when the MLD was shoaling, than between August and October, when changes in MLD were relatively small. In early August, the percent loss of production due to UVR was approximately four-fold greater at the ocean surface than when integrated over depth (Figure 13d), indicative of the deeply mixed water column. By December, however, the ratio of surface loss to depth-integrated loss dropped to <1.7 due to the summertime reduction in MLD. The 20–55% loss of depth-integrated production predicted here due to UVR is similar to the losses of 15–40% reported by *Boucher and Prézelin* [1996] for the Antarctic Peninsula LTER site and <10 to >50% estimated for the Weddell-Scotia Confluence [*Neale et al.*, 1998a, 1998b]. It should be noted, however, that these estimates are based on a combination of field and/or laboratory work and modeling. When in situ deployments alone are used to determine the impact of UVR on integrated productivity, the losses in primary production due to UVR are lower, generally <15% [e.g., *Holm-Hansen et al.*, 1993]. This may be due in part to the fact that phytoplankton assemblages in coastal waters, where most in situ deployments take place, appear to be less sensitive to UVR than those located offshore.

[34] As was seen at Station A on 4 October, most of the inhibition by UVR was due to UVA. Unfortunately, the model employed for this study does not permit a calculation of the exact fraction of total UVR inhibition attributable to either UVA or to UVB. Although H_{inh} (which ultimately determines the UVR-inhibited rate of production) can easily be separated into components controlled by UVA and by UVB, B_{eff} can not. This is because of the nonlinear response by B_{eff} to changes in H_{inh} (equation (7a)). For example, if H_{inh} calculated from 280–320 nm is 0.08 and H_{inh} between 320 and 400 nm is 0.21, then H_{inh} for 280–400 nm will simply be 0.29. However, a value for H_{inh} of 0.08 (for UVB) results in a calculated B_{eff} of 0.92, which according to equation (5) will reduce production by 8%. A value of H_{inh} for UVA of 0.21 yields a B_{eff} of 0.81 and a 19% reduction in production. If the UVA and UVB values for H_{inh} are summed (0.29), a B_{eff} of 0.74 and a corresponding loss of production of 26% results. Clearly, while the values for H_{inh} are additive (0.21 for UVA plus 0.08 for UVB equals 0.29 for UVA + B), the resulting losses in production calculated from B_{eff} are not (19% for UVA plus 8% for UVB does not

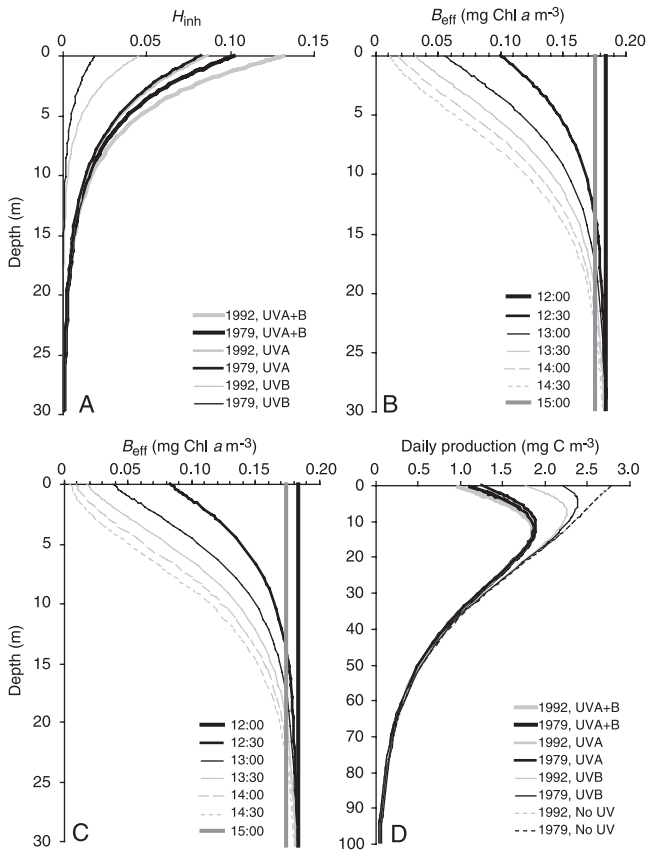

Figure 12. Effect of UVR on primary production throughout the euphotic zone. Vertical profiles of (a) H_{inh} at noon showing the relative contributions by UVA and UVB, (b) changes in calculated B_{eff} between noon and 15:00 hours for 1979 and (c) 1992, and daily production for 1979 and 1992 under different UVR regimes. In the case of B_{eff} shown in Figures 12b and 12c, T_{mix} was set to 3 hours and the 15:00 hours profile was obtained by "mixing" (actually averaging) B_{eff} from the previous time step (approximated by the curve for 02:30) over the entire MLD, in this case 220 m. All profiles were from October 4 at Station A.

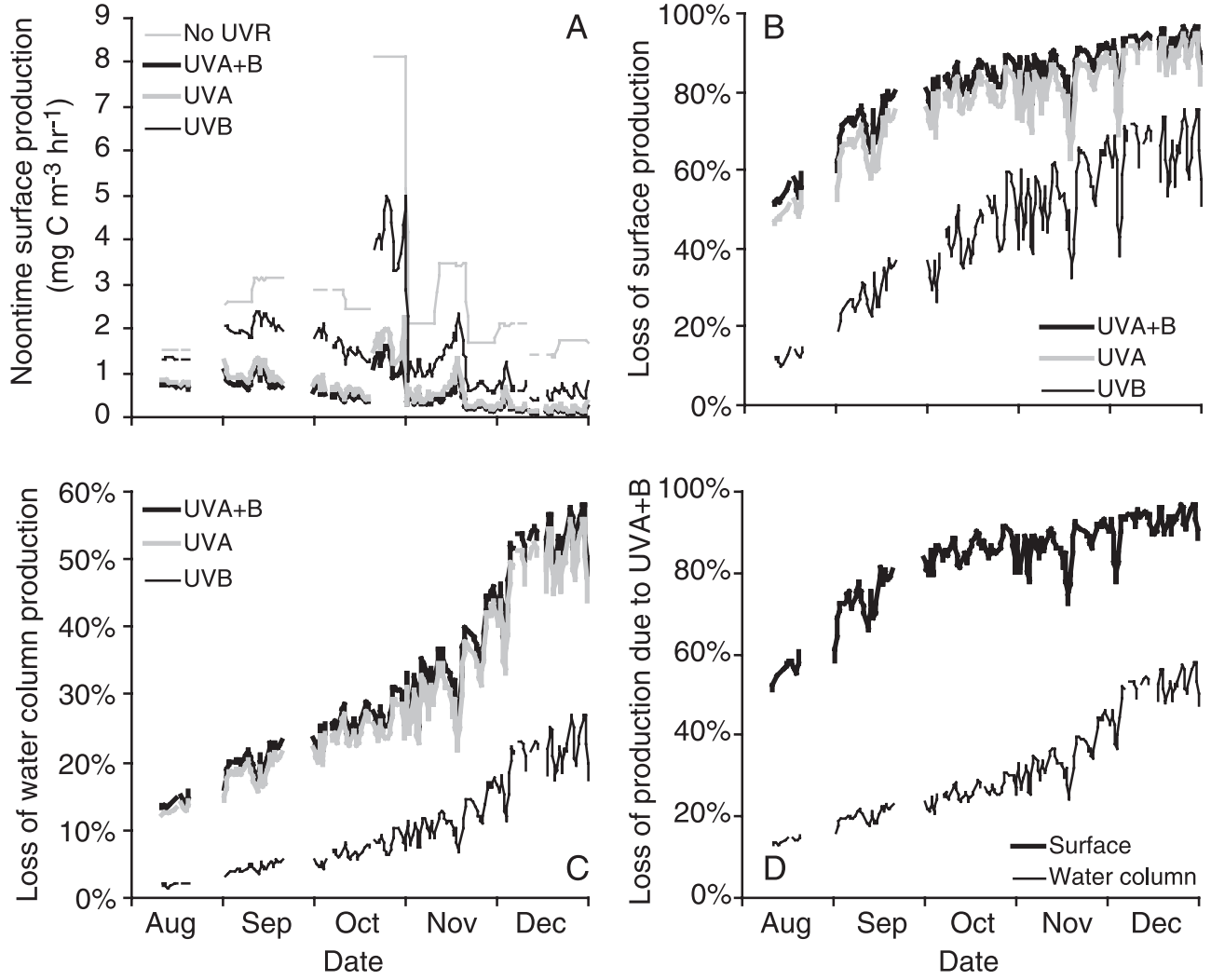

Figure 13. Temporal variations at Station A in (a) the impact of UVA + B, UVB, and UVA on surface primary production at noon, (b) the loss of surface production resulting from UVA + B, UVB, and UVA, (c) the loss of water column production resulting from UVA + B, UVB, and UVA, and (d) the loss of production at the surface and throughout the water column as a function of UVA + B. All time series are for 1979 at Station A.

equal 26% for UVA+B). The effect is amplified as a new B_{eff} is calculated at each successive 5-min time step, and explains how on 4 October, UVB and UVA could result in a 26.7% and 68.4% loss of production, respectively, while the loss due to both combined (UVA + B) is only slightly greater (73.9%) than for UVA alone (Figure 13b). Field measurements also indicate that UVA is responsible for most of the inhibition by UVR [e.g., *Neale et al.*, 1998a, 1998b] and our estimate of >60% loss of production due only to UVA is similar to the values of 60% measured by *Helbling et al.* [1992] and 67% observed by *Holm-Hansen et al.* [1993].

[35] Although depth-integrated losses of production due to UVR inhibition were large in both 1979 and 1992, the differences in production at Station A between 1979 and 1992 were <2% (Figure 14a), and averaged only 0.7%. Not surprisingly, the seasonal pattern of production differences between 1979 and 1992 reflected the changes in O_3 concentration, with a correlation coefficient of 0.91. O_3 was almost always lower in 1992 than in 1979, in some cases by >60%, but averaging approximately 23%. Despite the relatively large decreases in O_3, depth-integrated production was changed very little. The ratio of the percent loss in production between 1979 and 1992 to the percent decrease in O_3 over the same time frame suggests that for each 10% loss in O_3, an additional 0.1–0.5% loss of primary production can be expected at Station A, depending upon the time of year (Figure 14b). This temporal increase in the sensitivity of primary production to changes in O_3 is the result of increasing solar insolation. That is, for a given change in O_3, the flux of UVB, and consequently the degree of inhibition, will be greater in December than in August.

3.2.3. Seasonal Cycle of Production Throughout the Southern Ocean

[36] The change of production resulting from the O_3 differences between 1979 and 1992 exhibited spatial variation related to interannual differences in O_3 abundance

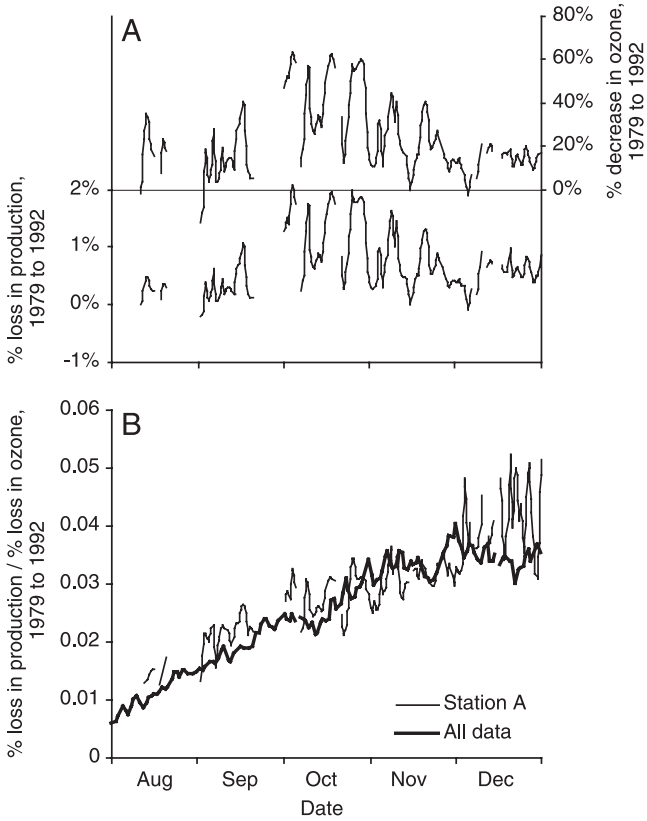

Figure 14. (a) Temporal variations in the loss in primary production and the decrease in ozone between 1979 and 1992 at Station A, and (b) the ratio of the loss in primary production between to the decrease in ozone between 1979 and 1992 at Station A and over the model domain.

(Figure 15). On 1 August, spatial variability was lowest, with changes in production between 1979 and 1992 ranging from +0.25% to −0.5% across the Southern Ocean. Positive values indicate that productivity in 1992 was actually greater than in 1979, although these are restricted to those few areas where 1992 O_3 concentrations were greater than in 1979 (e.g., northwest of the Antarctic Peninsula). Spatial variability was greatest during October when the O_3 hole was at its peak; changes in production between 1979 and 1992 on 1 October ranged from +0.5% in the Pacific sector of the Southern Ocean to −2.0% in the southern Indian Ocean. These losses in depth-integrated production due to the O_3 hole are similar to, although somewhat smaller than, previous estimates of 3.8% based on field data [*Holm-Hansen et al.*, 1993] and 2.7–5% estimated using a combination of field data and assuming a 50% reduction in O_3 [*Boucher and Prézelin*, 1996; *Neale et al.*, 1998a]. Our lower estimate reflects the fact that mean O_3 losses over open water between 1979 and 1992 were less than those experienced during the study by *Holm-Hansen et al.* [1993] and far less than the 50% used in calculations by *Boucher and Prézelin* [1996] and *Neale et al.* [1998a] (Figure 7a).

[37] The time series of spatial mean production for 1979 and 1992 are virtually indistinguishable when plotted together (Figure 16a), ranging from <50 mg C m^{-2} d^{-1} in early August to >275 mg C m^{-2} d^{-1} in December. The spatial mean loss of depth-integrated production between 1979 and 1992 ranged from 0% in August to 0.5% in December (Figure 16b). This corresponds to a primary production loss of 0.25% or 7 Tg C for all waters south of 50°S and 1 Tg C in the MIZ, using primary production estimates for the months of August through December from *Arrigo et al.* [1998a]. This value is significantly lower than the previously estimated loss of production in the MIZ due to O_3 depletion of 2–4% [*Smith et al.*, 1992], which is equivalent to a loss of 8–17 Tg C assuming an annual production rate in the Antarctic MIZ of 422 Tg C [*Arrigo et al.*, 1998a].

[38] When averaged over the entire Southern Ocean, the correlation between percent loss of production from 1979 to 1992 and the percent decrease in O_3 from 1979 to 1992 was 0.85, slightly less than the value of 0.91 obtained at Station A. Because these are model results, one might expect a perfect correlation between decreased O_3 concentration and loss of depth-integrated primary production. The correlation coefficient is <1.0, however, because other factors can modulate the effect of diminishing O_3 concentration on rates of primary production. For example, as stated earlier,

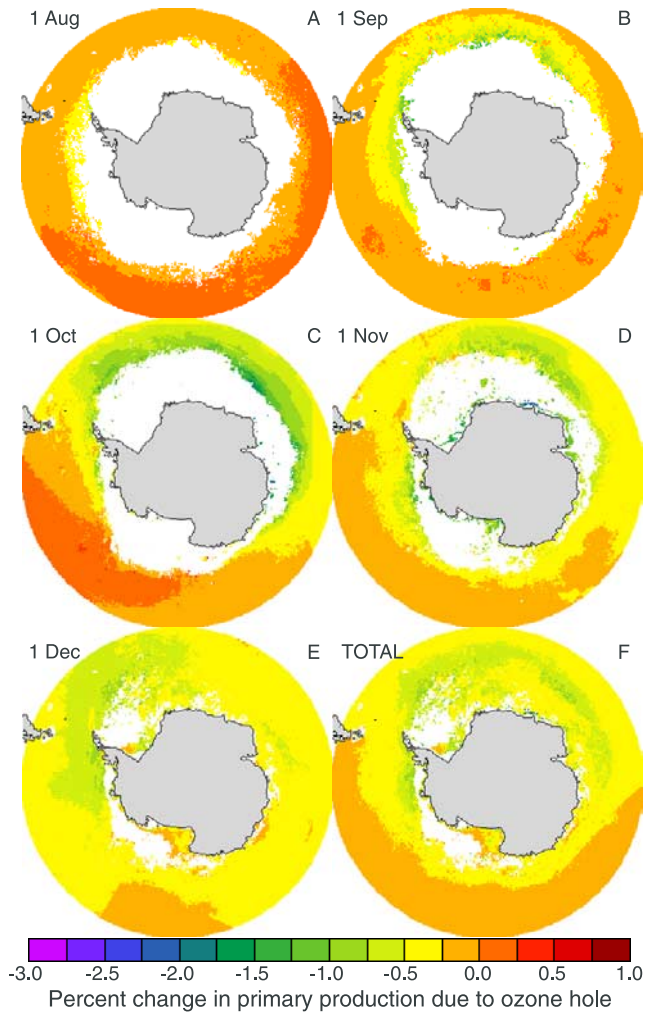

Figure 15. Temporal variations in the percent change in primary production between 1979 and 1992 within our study area. TOTAL (Figure 15f) refers to the period August through December.

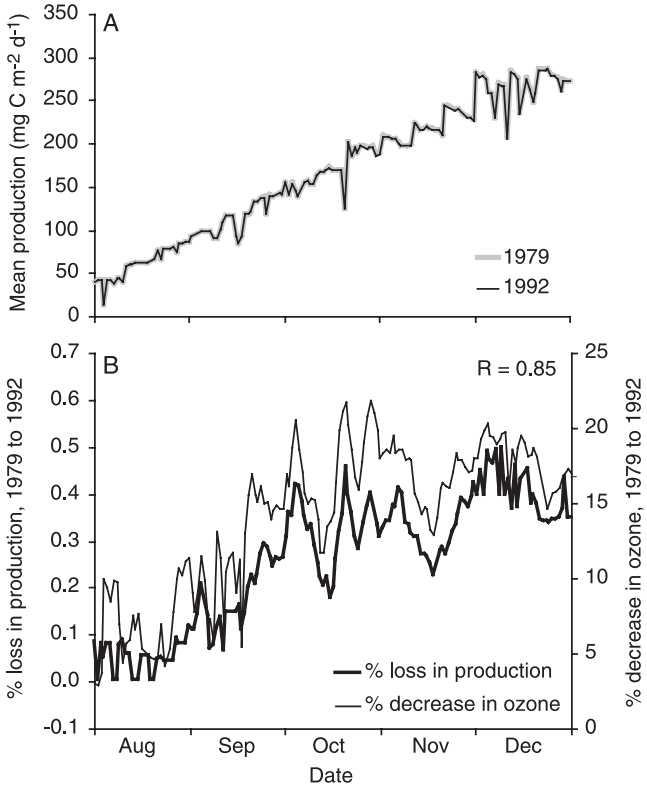

Figure 16. Temporal variations in (a) mean primary production for 1979 and 1992 within our study area and (b) the mean loss in primary production and the decrease in ozone between 1979 and 1992 within our study area.

a similar decrease in O_3 concentration at two different times of the year will result in different UVB fluxes, and consequently, different production estimates. Similarly, MLD and the concentrations of light absorbing substances such as Chl *a*, CDOM and detritus can all modify the effects of decreased O_3. These appear to be second order effects, however, and changes in O_3 exert the strongest influence on losses of production between 1979 and 1992.

3.3. Sensitivity Analyses

[39] The model used in the present study contains a large number of parameters, most of which have some degree of natural variability that has not been accounted for in the standard model run. Therefore, it was imperative that a sensitivity analysis be performed to understand the potential impact that variation in these parameters can have on the results presented here. All the relevant parameters used in equations (4)–(7) were tested, as well as T_{mix} and MLD. The analysis is presented only for 4 October at Station A when the O_3 difference between 1979 and 1992 was large; model sensitivity was lower at other times and locations.

3.3.1. MLD and T_{mix}

[40] The standard run of the model simulated complete mixing of the MLD (= 220 m on 4 October at Station A) every 3 hours. Changing the MLD had very little effect on the calculated difference in production between 1979 and 1992, except when T_{mix} was less than 3 hours (Figure 17a). Under those circumstances, changes in T_{mix} and MLD resulted in the largest deviations from the standard run of all the parameters tested. However, even in the most extreme case with a MLD of 40 m and T_{mix} of 0.5 hours, a mixing time probably too short for a 40 m MLD [*Denman and Gargett*, 1983], the loss in production between 1979 and 1992 increased only by a factor of 3, from 1.73% in the standard run to just over 5%. Including possible interactions between MLD and the biological weighting function could increase our maximum loss of production from 5% to 8% [*Neale et al.*, 1998a]. Assuming that all times and locations underestimate UVR inhibition by a similar degree (a gross exaggeration), the calculated loss of production over the Southern Ocean due to the O_3 hole would still be <1%.

3.3.2. Temperature Dependence of Primary Production

[41] The relationship between primary production and temperature is controlled by two coefficients given in equation (6). G_0 and k were both derived from the relationship of *Eppley* [1972] and describe, respectively, the net specific rate of change at 0°C and the speed at which this rate changes with temperature. Changes in these parameters affected the 1979 and the 1992 simulations equally; consequently, reducing or increasing either by as much as a factor of 10 had no effect on the amount of UVR inhibition of primary production due to the O_3 hole (Figure 17b). We do not account, however, for possible changes in photorepair processes that might change in response to temperature.

3.3.3. Photoacclimation Parameter

[42] The parameter E_k defines the light level at which photosynthesis is approximately saturated and is assumed to be 80 μEin m^{-2} s^{-1} of PUR in the model (or approximately 150 μEin m^{-2} s^{-1} of PAR depending on spectral attenuation within the water column). Decreasing E_k to 8 μEin m^{-2} s^{-1} decreased the impact of the O_3 hole on primary production

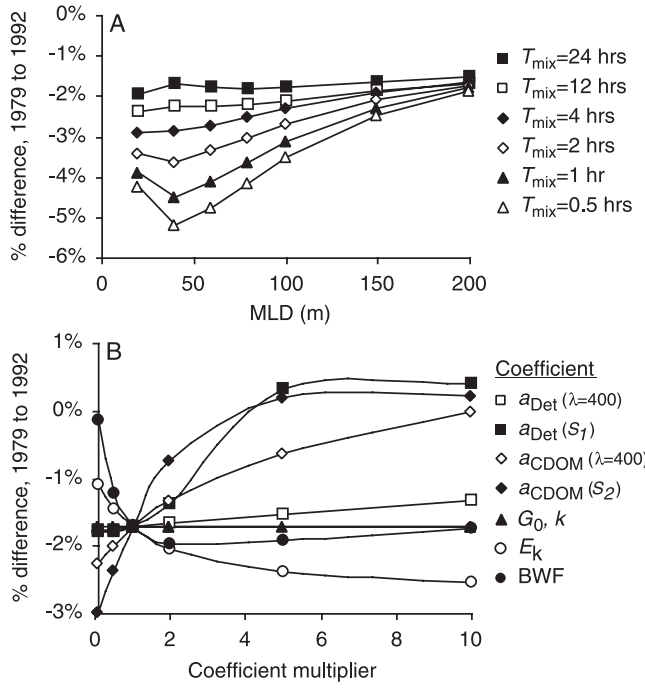

Figure 17. Sensitivity of the model to (a) changes in mixed layer depth (MLD) and T_{mix} and (b) various absorption and phytoplankton physiological parameters. See text for definition of parameters.

by allowing photosynthesis to saturate at much lower irradiance levels. This increased the relative contribution of deeper layers to total water column production, layers where UVR was unable to penetrate. Increasing E_k had the opposite effect, shifting production to shallower depths where UVR was relatively greater. Nevertheless, the estimated UV inhibition due to the O_3 hole at Station A increased only from 1.73% to approximately 2.5% in response to a 10-fold increase in E_k.

3.3.4. Detrital Absorption

[43] The shape of the detrital absorption spectra is determined by $a_{Det}(440)$ and S_1, terms which are defined in equation (4d). Altering the value for $a_{Det}(440)$ shifts the absorption spectra higher or lower, while changing S_1 results in an absorption spectra with either a steeper or more gradual spectral slope. Increasing S_1 while holding $a_{Det}(440)$ constant will increase detrital absorption in the UVR range while decreasing absorption in the visible. Simulations where either $a_{Det}(440)$ or S_1 were decreased by as much as a factor of 10 resulted in slightly more UVR inhibition of primary production than was predicted by the standard run (Figure 17b). This is because attenuation of UVR by detritus is reduced, allowing higher levels of UVR to reach the phytoplankton. Higher detrital absorption (increased $a_{Det}(440)$ and S_1) reduced, relative to the standard run, the amount of UVR inhibition due to the O_3 hole, but only slightly. In this case, increasing S_1 had a larger effect than changes in $a_{Det}(440)$, but even when $a_{Det}(440)$ was increased 10-fold, the productivity difference between 1979 and 1992 increased from −1.73% in the standard run to +0.4%. The positive sign indicates that production was actually higher in 1992, despite the lower O_3 abundance, and is a consequence of the photoprotective effect of enhanced detrital absorption [*Arrigo and Brown*, 1996]. The marginal effects of even large changes in CDOM absorption reflects the first-order importance of seawater in attenuating UVR with depth. Because seawater absorbs so strongly at these short wavelengths, even relatively large changes in detrital absorption have only a small influence on the flux of UVR.

3.3.5. CDOM Absorption

[44] The effects of changes in CDOM absorption on UVR inhibition of primary production were very similar to those elicited by changes in detrital absorption (Figure 17b). This is not surprising given the similarity between equation (4d), which describes spectral attenuation by detritus, and equation (4e), the attenuation by CDOM. Reducing either $a_{CDOM}(400)$ or S_2 resulted in a slightly higher level of UVR inhibition than did their detrital counterparts. However, in the most extreme case tested, a 10-fold decrease in S_2 increased UVR inhibition due to the O_3 hole from 1.73% in the standard run to <3%. As was the case for detrital absorption, dramatically increasing CDOM absorbance resulted in less UVR inhibition than the standard run, and the photoprotective effect of this resulted in slightly higher production in 1992 than in 1979. Nevertheless, the effect on rates of production of 10-fold changes in CDOM absorption and spectral shape was relatively small, changing the degree of UVR inhibition due of the O_3 hole by less than two-fold.

3.3.6. Phytoplankton Absorption

[45] To assess the effect of changes in the phytoplankton absorption spectra on estimates of UVR inhibition, only absorption values in the UVR range were modified (Figure 18a). The effects of three different absorption spectra were tested: the value used in the standard run, a high UVR absorption spectrum where absorption at 320 nm is approximately 2.5-fold greater than the standard run, and a low UVR absorption spectrum where absorption at 320 nm was greater than two-fold less than the standard run. The high and low UVR absorption spectra are consistent with extreme values found in the literature for the Southern Ocean [e.g., *Riegger and Robinson*, 1997; *Arrigo et al.*, 1998a]. Despite the large differences in UVR absorption between the three spectra tested, estimates of UVR inhibition due to reduced O_3 abundance were virtually unchanged from the standard run. Whereas productivity was reduced by 1.73% in the standard run, it was reduced by 1.66% and 1.75% in the high and low phytoplankton absorbance cases, respectively. While these differences would likely be larger in waters where Chl *a* concentrations are greater than those at Station A on 4 October, even if Chl *a* concentrations were reduced by a factor of 10 (to allow extra UVR penetration), the calculated degree of UVR inhibition due to the O_3 hole would still be <2% (compared to 1.73% in the standard run).

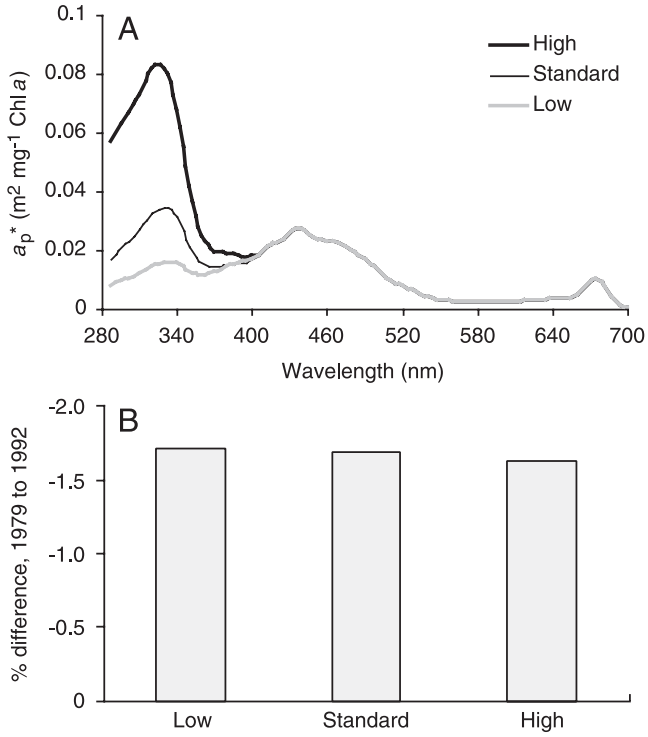

Figure 18. (a) Different phytoplankton absorption spectra used in sensitivity analyses, and (b) sensitivity of the model to changes in phytoplankton absorption within the UVR range.

3.3.7. BWF

[46] Because ε_H for UVR inhibition of phytoplankton productivity is variable in both spectral shape and magnitude [*Helbling et al.*, 1992; *Holm-Hansen et al.*, 1993; *Neale et al.*, 1998a], we tested the sensitivity of modeled depth-integrated productivity under O_3 hole and non-O_3 hole conditions to variability in the BWF. In the first

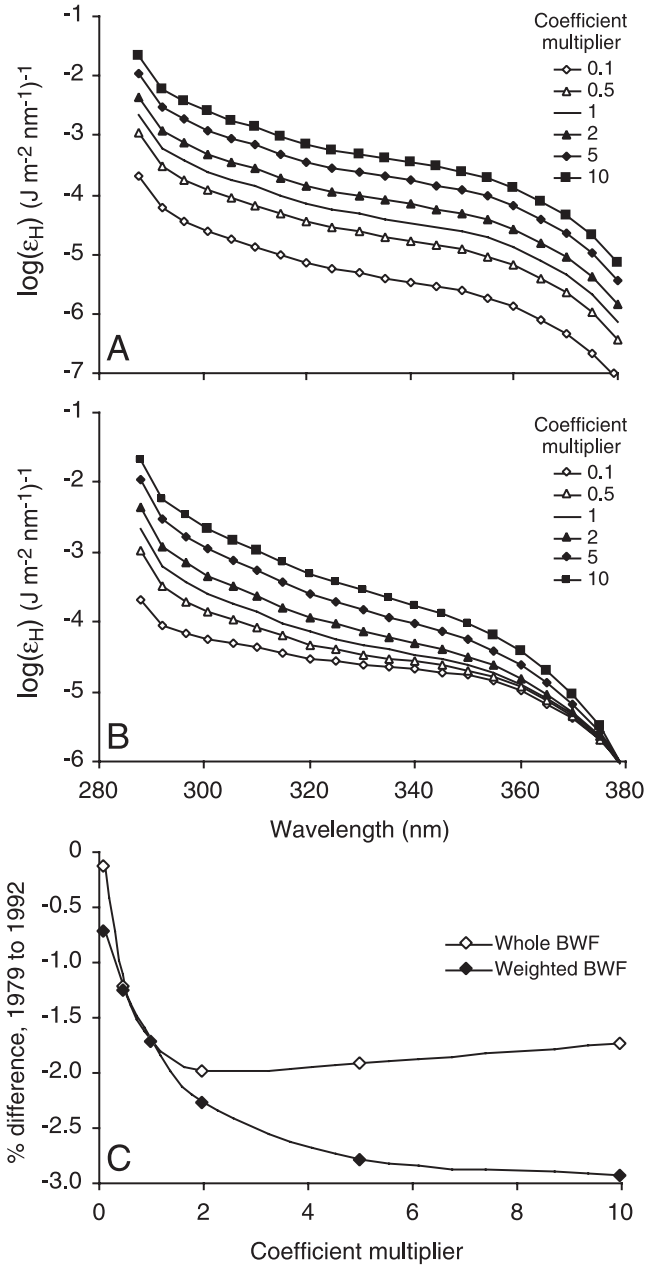

Figure 19. Changes made in the magnitude of the biological weighting function (BWF, ε_H) (a) keeping the spectral shape constant and (b) keeping only the value at 380 nm constant, and (c) sensitivity of the model to the changes made in the magnitude (whole) and spectral shape (weighted) of the BWF as shown in Figures 19a and 19b.

analysis, the BWF was multiplied by a scaling factor ranging from 0.1 to 10 but its spectral shape was maintained (Figure 19a). Lowering by 10-fold the phytoplankton sensitivity to UVR only reduced the degree of UVR inhibition from 1.73% to 0.13% (Figure 19c). A similar 10-fold increase in the magnitude of ε_H increased the difference in primary productivity between 1979 and 1992 from 1.73% to <2% (Figure 19c).

[47] In the second analysis, the spectral shape of the BWF was modified by multiplying the BWF at 280 nm by a scaling factor that varied from 0.1 to 10 while holding the value at 380 nm constant. This resulted in a weighted BWF with larger changes within the UVB range than in the UVA (Figure 19b). Again, the difference in productivity between an O_3 hole and non-O_3 hole year was small, <3% (compared to 1.73% in the standard run), regardless of the shape of the BWF. Although in reality a higher change in UVR sensitivity might be expected in the UVA range than in the UVB range [*Neale and Kieber*, 2000], this scenario would result in even smaller differences between 1979 and 1992 than the one we tested. These results suggest that unless the BWF is changing from year to year, the changes in production due to the O_3 hole will be small, regardless of the absolute degree of UVR sensitivity by the phytoplankton.

3.3.8. Instantaneous Versus Cumulative Exposure To UVR

[48] Finally, we studied the effect of using an instantaneous (rather than cumulative) formulation for UVR inhibition [*Cullen et al.*, 1992]. The only BWF of this kind available at the time of our study was from a diatom culture grown at 25°C and, therefore, the comparison should be treated with some skepticism. Nevertheless, when averaged over the entire Southern Ocean from August through December, this formulation predicted differences in primary production between 1979 and 1992 that were only approximately 50% of those obtained using the cumulative exposure approach. Therefore, if phytoplankton are responding to UVR exposure in a manner consistent with instantaneous model, the predicted loss of production due to the O_3 hole would be even less than the 0.25% predicted here.

4. Discussion

[49] Several factors contributed to the disparity between the severe stratospheric O_3 depletion and the minimal reduction in depth-integrated rates of primary production reported here. First, although UVB inhibition of photosynthetic rates is substantial near the ocean surface, UVB attenuates rapidly with depth, with a 10% penetration depth at 305 nm of <10 m. Consequently, there is relatively little UVB inhibition below 15 m, depths where primary productivity can represent a substantial fraction of the depth-integrated total in the Southern Ocean [*El-Sayed and Taguchi*, 1981].

[50] More importantly, the Antarctic O_3 hole is most extensive in September–October, when sea ice coverage is near maximal and rates of phytoplankton production are low. During the austral spring of 1992, less than 10% of the ice-free waters south of 50°S were beneath the O_3 hole at any time (Figure 7c). In September, only ~9% of ice-free waters were beneath the O_3 hole for more than 10 days and less than 3% for greater than 20 days (Figure 20a). By October, only 5% of ice-free waters were exposed to the O_3 hole for over 10 days and the maximum time of exposure for any location in that month was only 16 days (Figure 20b). Virtually no ice-free waters were exposed to the effects of the O_3 hole in November (Figure 20c) or December (Figure 20d), which are the months of highest production. Thus, the co-occurrence of the Antarctic O_3 hole with near-maximum sea ice extent reduced the potential for deleterious effects of

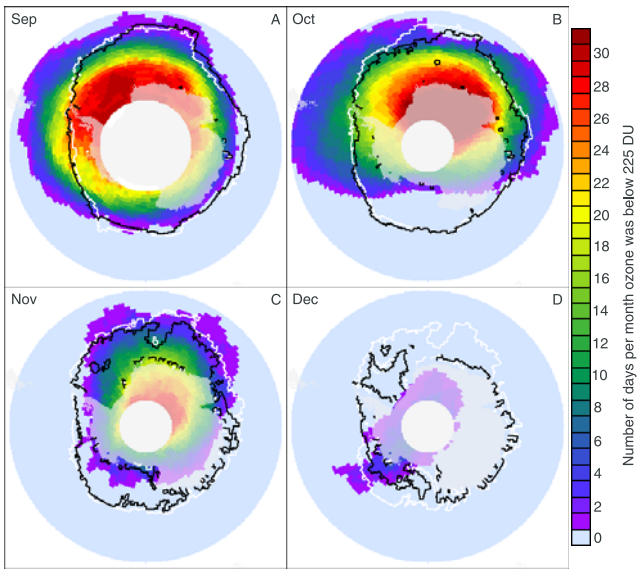

Figure 20. Spatial variation in the number of days in 1992 that ozone concentrations were below 225 DU (defined as an ozone hole) for the month of (a) September, (b) October, (c) November, and (d) December. The white and black lines denote the 50% contour of sea ice concentration on the first and last day, respectively, of each month.

enhanced UVB fluxes on phytoplankton production in the Southern Ocean. It is important to note, however, that recent O_3 holes have experienced similarly reduced O_3 concentrations but have persisted for longer periods of time and extended further north (see www.cpc.ncep.noaa.gov). Should these trends continue, phytoplankton will be exposed to increasingly intense UVR at higher solar elevations.

[51] Because the model presented here is a simplified representation of the ice-free areas of the Southern Ocean, there is some uncertainty associated with estimated losses of production resulting from the O_3 hole. Although difficult to quantify, virtually all of the simplifications made in the model result in overestimates of the calculated loss of phytoplankton production due to the Antarctic O_3 hole. For example, a minimum threshold of UVR exists below which UVR photorepair mechanisms keep pace with UVR damage without a reduction in photosynthetic rate [*Helbling et al.*, 1992]. In addition, some phytoplankton are able to acclimate to enhanced UVR within days of exposure [*Villafane et al.*, 1995]. Processes related to UVR photorepair and photoacclimation are not currently included in the model but would reduce the predicted magnitude of UVR inhibition. Consequently, because most model assumptions tend to maximize UVR inhibition, our estimates likely represent upper limits to O_3 hole-induced inhibition of primary production in Southern Ocean waters.

[52] One possible exception involves our choice of the pure water absorption spectrum of *Smith and Baker* [1981] over the more recently published version by *Pope and Fry* [1997]. Absorption of UVA and blue light in the *Pope and Fry* [1997] spectrum is considerably lower than that used here and would have allowed increased transmission of UVA to depth, and possibly greater UVR inhibition than we report. However, it must be noted that (1) the *Pope and Fry* [1997] spectrum ranges only from 380 to 700 nm and would be of limited value to this study, and (2) the CDOM absorption spectrum used here [*Arrigo et al.*, 1998a] was obtained by measuring absorption by CDOM + pure water and then subtracting the pure water absorption reported by *Smith and Baker* [1981]. Therefore, using the reduced *Pope and Fry* [1997] spectrum would require adjustment of our CDOM absorption spectrum upwards to compensate for their lower pure water absorption (CDOM + pure water absorption was fixed by the field data). This adjustment would result in no net change in the underwater irradiance field, and therefore, the choice of pure water absorption spectrum had no effect on our results.

[53] Sensitivity analyses show that even large (10-fold) changes in the model coefficients would not alter the general conclusion that losses of production due to the O_3 hole are less than a few percent. This should not be interpreted to mean that UVR is having little effect of rates of primary production in the Southern Ocean. The model predicts large losses of production as a result of the flux of UVR, particularly in surface waters where the flux of UVR is greatest. In some cases, these losses exceed 90% relative to simulations where UVR is removed. However, it must be remembered that large losses of production are being sustained under conditions of both high and low O_3 abundance and that the incremental losses due to changes in O_3 associated with the O_3 hole are much smaller than 90%, even in surface waters. When integrated over depth, the percent loss of production due to the O_3 hole disappears almost completely.

[54] Our results suggest that increased UVR due to springtime Antarctic O_3 depletion has only a small impact (<0.25%) on marine primary production during the months of August through December. The O_3-related losses of primary production in the Southern Ocean for the entire year (all 12 months) would be much less than our figure of 0.25% for the following reasons: (1) Sea ice cover usually reaches its minimum in February so the area of open water will be at maximal at this time, (2) phytoplankton standing stocks in the months of January through May are at least equal to that in the months August through December [*Clarke*, 1988; *Arrigo et al.*, 1998b], (3) because there is no O_3 hole in the months January–May, there are no losses of primary production due to enhanced UVB radiation during that time period, and (4) our estimates exclude primary production associated with sea ice, for which UVB losses would be less than for open surface waters due to the rapid attenuation of the shorter UVB wavelengths by sea ice. Taking all these factors into consideration, the estimated loss of total annual primary production in the Southern Ocean by enhanced UVB radiation would be <0.12%. This value is consistent with the earlier estimate of 0.20% based on in situ incubation data [*Holm-Hansen et al.*, 1993] but more than an order of magnitude lower than the 2–4% loss in annual primary production in the MIZ calculated by *Smith et al.* [1992]. Although it has been suggested that enhanced UVR associated with the O_3 hole may pose a threat to the Antarctic food web and potentially result in the loss of fish production [*Häder et al.*, 1994], our results suggest that the loss of primary production is too

small to have a serious impact on the Antarctic marine ecosystem.

[55] It should be noted, however, that there may be other important consequences of enhanced UVB fluxes other than direct effects on primary production. These include (1) changes in phytoplankton species composition due to differential photoprotection (e.g., screening by micosporine-like amino acids) and repair mechanisms (e.g., photoreactivation) in response to enhanced UVR [*Karentz*, 1994], (2) changes in phytoplankton population structure that could result in modifications of the marine food web [*Davidson et al.*, 1996] as well as altering patterns of nutrient utilization [*Arrigo et al.*, 1999] and C export flux [*DiTullio et al.*, 2000], and (3) deleterious effects on any life stage of heterotrophic organisms found in surface waters (e.g., fish eggs) or in shallow benthic environments. Such ecological implications of enhanced UVR fluxes, besides diminished photosynthetic rates, should be a major focus of future research.

[56] **Acknowledgments.** This work was supported primarily by NASA grant NAG5-6414. Development of the atmospheric radiative transfer algorithm was also supported in part by the NASA Atmospheric Chemistry Modeling and Analysis Program under NAG5-8252. We would like to thank P. Neale for providing the BWF data.

References

Allison, I., R. E. Brandt, and S. G. Warren, East Antarctic sea ice: Albedo, thickness distribution, and snow cover, *J. Geophys. Res.*, *98*, 12,417–12,429, 1993.

Arrigo, K. R., Impact of ozone depletion on phytoplankton growth in the Southern Ocean: Large scale spatial and temporal variability, *Mar. Ecol. Prog. Ser.*, *114*, 1–12, 1994.

Arrigo, K. R., and C. W. Brown, Impact of chromophoric dissolved organic matter on UV inhibition of primary productivity in the sea, *Mar. Ecol. Prog. Ser.*, *140*, 207–216, 1996.

Arrigo, K. R., D. H. Robinson, M. P. Lizotte, D. L. Worthen, and B. Schieber, Bio-optical properties of the southwestern Ross Sea, *J. Geophys. Res.*, *103*, 21,683–21,695, 1998a.

Arrigo, K. R., D. L. Worthen, A. Schnell, and M. P. Lizotte, Primary production in Southern Ocean waters, *J. Geophys. Res.*, *103*, 15,587–15,600, 1998b.

Arrigo, K. R., D. H. Robinson, D. L. Worthen, R. B. Dunbar, G. R. DiTullio, M. VanWoert, and M. P. Lizotte, Phytoplankton community structure and the drawdown of nutrients and CO_2 in the Southern Ocean, *Science*, *283*, 365–367, 1999.

Boucher, N. P., and B. B. Prézelin, Spectral modeling of UV inhibition of in situ Antarctic primary production using a field-derived biological weighting function, *Photochem. Photobiol.*, *64*, 407–418, 1996.

Briegleb, B. P., Delta-Eddington approximation for approximation for solar radiation in the NCAR community climate model, *J. Geophys. Res.*, *97*, 7603–7612, 1992.

Burt, W. V., Albedo over wind-roughened water, *J. Meteorol.*, *11*, 283–289, 1954.

Cavalieri, D. J., P. Gloersen, C. L. Parkinson, J. C. Comiso, and H. J. Zwally, Observed hemispheric asymmetry in global sea ice changes, *Science*, *278*, 1104–1106, 1997.

Clarke, A., Seasonality in the Antarctic marine environment, *Comput. Biochem. Physiol.*, *90B*, 461–473, 1988.

Cullen, J. J., P. J. Neale, and M. P. Lesser, Biological weighting function for the inhibition of phytoplankton photosynthesis by ultraviolet radiation, *Science*, *258*, 646–650, 1992.

Davidson, A. T., H. J. Marchant, and W. K. de la Mare, Natural UVB exposure changes the species composition of Antarctic phytoplankton in mixed culture, *Aquatic Microbiol. Ecol.*, *10*, 299–305, 1996.

Denman, K. L., and A. E. Gargett, Time and space scales of vertical mixing and advection of phytoplankton in the sea, *Limnol. Oceanogr.*, *28*, 801–815, 1983.

DiTullio, G., R. J. Grebmeier, K. R. Arrigo, M. P. Lizotte, D. H. Robinson, A. Leventer, J. Barry, M. VanWoert, and R. B. Dunbar, Rapid and early export of Phaeocystis antarctica blooms in the Ross Sea, Antarctica, *Nature*, *404*, 595–598, 2000.

Eck, T. F., P. K. Bhartia, P. H. Hwang, and L. L. Stowe, Reflectivity of Earth's surface and clouds in ultraviolet from satellite observations, *J. Geophys. Res.*, *92*, 4287–4296, 1987.

El-Sayed, S. Z., and S. Taguchi, Primary production and standing crop of phytoplankton along the ice-edge in the Weddell Sea, *Deep Sea Res.*, *28*, 1017–1032, 1981.

Eppley, R. W., Temperature and phytoplankton growth in the sea, *Fish. Bull.*, *70*, 1063–1085, 1972.

Frederick, J. E., and H. E. Snell, Ultraviolet-radiation levels during the Antarctic Spring, *Science*, *241*, 438–440, 1988.

Gregg, W. W., and K. L. Carder, A simple spectral solar irradiance model for cloudless maritime atmospheres, *Limnol. Oceanogr.*, *35*, 1657–1675, 1990.

Häder, D.-P., R. C. Worrest, H. D. Kumar, and R. C. Smith, Effects of increased solar ultraviolet radiation on aquatic ecosystems, in *Environmental Effects of Ozone Depletion: 1994 Assessment*, pp. 65–78, U. N. Environ. Programme (UNEP), London, 1994.

Helbling, E. W., V. Villafane, M. Ferrario, and O. Holm-Hansen, Impact of natural ultraviolet radiation on rates of photosynthesis and on specific marine phytoplankton species, *Mar. Ecol. Prog. Ser.*, *92*, 89–100, 1992.

Herman, J. R., and D. Larko, Low ozone amounts during 1992–1993 from NIMBUS 7 and METEOR 3 Total Ozone Mapping Spectrometers, *J. Geophys. Res.*, *99*, 3483–3496, 1994.

Herman, J. R., N. Krotkov, E. Celarier, D. Larko, and G. Labow, Distribution of UV radiation at the Earth's surface from TOMS-measured UV-backscattered radiances, *J. Geophys. Res., 104*, *104*, 12,059–12,076, 1999.

Holm-Hansen, O., Short- and long-term effects of UVA and UVB on marine phytoplankton productivity, *Photochem. Photobiol.*, *65*, 266–268, 1997.

Holm-Hansen, O., E. W. Helbling, and D. Lubin, Ultraviolet-radiation in Antarctica: Inhibition of primary production, *Photochem. Photobiol.*, *58*, 567–570, 1993.

Joseph, J. H., W. J. Wiscombe, and J. A. Weinman, Delta-Eddington approximation for radiative flux transfer, *J. Atmos. Sci.*, *33*, 2452–2459, 1976.

Karentz, D., Ultraviolet tolerance mechanisms in Antarctic marine organisms, *Antarct. Res. Ser.*, *62*, 93, 1994.

Levitus, S., and T. Boyer, *World Ocean Atlas 1994,* vol. 4, *Temperature, NOAA Atlas NESDIS 4*, Natl. Oceanic and Atmos. Admin., Silver Spring, Md., 1994.

Lubin, D., and E. H. Jensen, Effects of clouds and stratospheric ozone depletion on ultraviolet-radiation trends, *Nature*, *377*, 710–713, 1995.

Lubin, D., J. E. Frederick, C. R. Booth, T. B. Lucas, and D. A. Neuschuler, Measurements of enhanced springtime ultraviolet radiation at Palmer Station, Antarctica, *Geophys. Res. Lett.*, *16*, 783–785, 1989.

Lubin, D., E. H. Jensen, and H. P. Gies, Global surface ultraviolet radiation climatology from TOMS and ERBE data, *J. Geophys. Res.*, *103*, 26,061–26,091, 1998.

Markus, T., Results from an ECMWF-SSM/I forced mixed layer model of the Southern Ocean, *J. Geophys. Res.*, *104*, 15,603–15,620, 1999.

Mitchell, B. G., and O. Holm-Hansen, Bio-optical properties of Antarctic peninsula waters: differentiation from temperate ocean models, *Deep Sea Res.*, *38*, 1009–1028, 1991.

Morel, A., Available, usable, and stored radiant energy in relation to marine photosynthesis, *Deep Sea Res.*, *25*, 673–688, 1978.

Neale, P. J., and D. J. Kieber, Assessing biological and chemical effects of UV in the marine environment: Spectral weighting functions, in *Causes and Environmental Implications of Increased U. V.-B., Radiation*, edited by R. E. Hester and R. M. Harrison, *R. Soc. Chem.*, *14*, 61–83, 2000.

Neale, P. J., R. F. Davis, and J. J. Cullen, Interactive effects of ozone depletion and vertical mixing on photosynthesis of Antarctic phytoplankton, *Nature*, *392*, 585–589, 1998a.

Neale, P. J., J. J. Cullen, and R. F. Davis, Inhibition of marine photosynthesis by ultraviolet radiation: Variable sensitivity of phytoplankton in the Weddell-Scotia Confluence during the austral spring, *Limnol. Oceanogr.*, *43*, 433–448, 1998b.

Pope, R. M., and E. S. Fry, Absorption spectrum (380–700 nm) of pure water: 2. Integrating cavity measurements, *Appl. Opt.*, *36*, 8710–8723, 1997.

Prézelin, B. B., N. P. Boucher, and R. C. Smith, Marine primary production under the influence of the Antarctic ozone hole: Icecolors '90, *Antarct. Res. Ser.*, *62*, 159, 1994.

Riegger, L., and D. Robinson, Photoinduction of UV-absorbing compounds in Antarctic diatoms and *Phaeocystis antarctica*, *Mar. Ecol. Prog. Ser.*, *160*, 13–25, 1997.

Sathyendranath, S., and T. Platt, Remote sensing of ocean chlorophyll: Consequences of non-uniform pigment profile, *Appl. Opt.*, *28*, 490–495, 1989.

Smith, R. C., and K. S. Baker, Optical properties of the clearest natural waters (200–800nm), *Appl. Opt.*, *20*, 177–184, 1981.

Smith, R. C., et al., Ozone depletion: Ultraviolet radiation and phytoplankton biology in Antarctic waters, *Science*, *255*, 952–959, 1992.

Stamnes, K., Z. Jin, J. Slusser, C. R. Booth, and T. B. Lucas, Several-fold enhancement of biologically effective ultraviolet radiation levels at McMurdo Station Antarctica during the 1990 ozone "hole," *Geophys. Res. Lett.*, *19*, 1013–1016, 1992.

Vernet, M., E. A. Brody, O. Holm-Hansen, and B. G. Mitchell, The response of Antarctic phytoplankton to ultraviolet radiation: Absorption, photosynthesis, and taxonomic composition, *Antarct. Res. Ser.*, *62*, 143–158, 1994.

Villafane, V., E. W. Helbling, O. Holm-Hansen, and B. E. Chalker, Acclimatization of Antarctic natural phytoplankton assemblages when exposed to solar ultraviolet radiation, *J. Plankton Res.*, *17*, 2295–2306, 1995.

K. Arrigo and G. L. van Dijken, Department of Geophysics, Stanford University, Stanford, CA 94305-2215, USA. (arrigo@stanford.edu; gertvd@pangea.stanford.edu)

O. Holm-Hansen, Marine Research Division, Scripps Institution of Oceanography, University of California, San Diego, La Jolla, CA 92093-0202, USA. (oholmhansen@ucsd.edu)

D. Lubin and E. Morrow, California Space Institute, Scripps Institution of Oceanography, University of California, San Diego, La Jolla, CA 92093-0221, USA. (dlubin@ucsd.edu; emorrow@arcane.ucsd.edu)